Published in final edited form as:
Geol Mag. 2019 June 17; N/A: . doi:10.1017/S0016756819000293.

Sedimentology and chemostratigraphy of the terminal Ediacaran Dengying Formation at the Gaojiashan section, South China

Huan Cui[1,2,3,4,*], **Shuhai Xiao**[5], **Yaoping Cai**[6], **Sara Peek**[4,7], **Rebecca E. Plummer**[4,8], **Alan J. Kaufman**[4,9]

[1] Research Group of Analytical, Environmental and Geo- Chemistry (AMGC), Division of Earth System Science, Vrije Universiteit Brussel (VUB), Brussels 1050, Belgium

[2] ET-HOME (Evolution and Tracers of the Habitability of Mars and Earth) Astrobiology Research Consortium, Belgium

[3] NASA Astrobiology Institute, Department of Geoscience, University of Wisconsin-Madison, Madison, Wisconsin 53706, USA

[4] Department of Geology, University of Maryland, College Park, MD 20742, USA

[5] Department of Geosciences, Virginia Tech, Blacksburg, VA 24061, USA

[6] State Key Laboratory of Continental Dynamics, Shaanxi Key Laboratory of Early Life and Environment, Department of Geology, Northwest University, Xi'an 710069, China

[7] United States Geological Survey, Menlo Park, CA 94025, USA

[8] Hydrology and Remote Sensing Laboratory, Beltsville Agricultural Research Center, US Department of Agriculture, Beltsville, MD 20705 USA

[9] Earth System Science Interdisciplinary Center, University of Maryland, College Park, MD 20742, USA

Abstract

The late Ediacaran Dengying Formation (ca. 551.1–538.8 Ma) in South China is one of two successions where Ediacara-type macrofossils are preserved in carbonate facies along with skeletal fossils and bilaterian animal traces. Given the remarkable thickness of carbonate-bearing strata deposited in less than 12.3 million years, the Dengying Formation holds the potential for a relatively continuous chemostratigraphic profile for the terminal Ediacaran stage. In this study, a detailed sedimentological and chemostratigraphic ($\delta^{13}C_{carb}$, $\delta^{18}O_{carb}$, $\delta^{13}C_{org}$, $\delta^{34}S_{pyrite}$, and $^{87}Sr/^{86}Sr$) investigation was conducted on the Dengying Formation at the Gaojiashan section, Ningqiang County of the southern Shaanxi Province, South China. Sedimentological results reveal an overall shallow marine depositional environment. Carbonate breccia, void-filling botryoidal precipitates, and aragonite crystal fans are common in the Algal Dolomite Member of the Dengying Formation, suggesting that peritidal facies were repeatedly karstified. The timing of karstification was likely early, probably soon after the deposition of the dolomite sediments. The presence of authigenic aragonite cements suggests high alkalinity in the terminal Ediacaran ocean.

[*]Author for correspondence: Huan.Cui@vub.be (H. Cui) or geohcui@gmail.com (H. Cui), Present address: Research Group of AMGC, Free University of Brussels (VUB), Brussels 1050, Belgium.

Geochemical analysis of micro-drilled samples shows that distinct compositions are registered in different carbonate phases, which should be considered when constructing chemostratigraphic profiles representative of true temporal variations in seawater chemistry. Integrated chemostratigraphic data suggest enhanced burial of organic carbon and pyrite, and the occurrence of extensive marine anoxia (at least in the Gaojiashan Member). Rapid basinal subsidence and carbonate accumulation during a time of elevated seawater alkalinity and increased rates of pyrite burial may have facilitated the evolutionary innovation of early biomineralizing metazoans.

Keywords

Geobiology; Animal biomineralization; Authigenesis; Aragonite; Karstification; Alkalinity; *Cloudina*

1. Introduction

The Ediacaran Period (ca. 635.2–538.8 Ma) witnessed the first rise of macroscopic, mobile, and biomineralizing animal life in Earth's history (Narbonne et al., 2012; Xiao et al., 2016). Ediacara-type macrofossils are primarily preserved as soft-bodied impressions in fine-grained siliciclastic rocks (Narbonne, 2005). However, these lithologies offer limited opportunities for paleoenvironmental analysis using geochemical tools. Two rare Ediacara-type macrofossil assemblages have thus far been found in well-preserved marine carbonate successions: the Khatyspyt Formation in Arctic Siberia (Fedonkin, 1990; Knoll et al., 1995; Grazhdankin et al., 2008; Rogov et al., 2012; Rogov et al., 2013a; Rogov et al., 2013b; Nagovitsin et al., 2015; Rogov et al., 2015; Cui et al., 2016a) and the middle Dengying Formation (Gaojiashan or Shibantan members) in South China (Sun, 1986; Xiao et al., 2005; Chen et al., 2014; Cui et al., 2016b; Mason et al., 2017; Shen et al., 2017; Chen et al., 2018). Insofar as both exhibit extraordinary fossils with exceptional preservation, these Lagerstätten provide unique windows into terminal Ediacaran ecosystems.

One of the foci of ongoing research in the Ediacaran Period is its subdivision using integrative stratigraphic tools (Narbonne et al., 2012; Xiao et al., 2016; Zhou et al., 2018). In particular, defining the terminal Ediacaran stage (TES) and its GSSP (Global Boundary Stratotype Section and Point) is a priority for the Subcommission on Ediacaran Stratigraphy (Xiao et al., 2016). In this regard, the terminal Ediacaran Dengying Formation at the Gaojiashan section (referred to "DYF@GJS" hereafter) can offer key insights leading to the eventual establishment of the TES, and may represent a viable candidate for the GSSP (see details in Section 2).

In this study, we conducted a high-resolution chemostratigraphic investigation of the 631.5 m thick DYF@GJS, including the Algal Dolomite and Beiwan members that we have not investigated in detail in previous studies (Figs. 1–12), in order to (1) complete its chemostratigraphic profile (Fig. 13) based on our earlier publication (Cui, 2015; Cui et al., 2016b); (2) evaluate the impact of diagenesis on various lithofacies preserved in the succession; (3) better constrain the environmental context of the carbonate platform, and (4) explore the potential causal link between paleoenvironmental change and early animal biomineralization during the terminal Ediacaran stage.

2. Significance the Dengying Formation

The Dengying Formation in this region has a number of features that may aid in the eventual establishment of the terminal Ediacaran stage (TES), which are summarized below.

Biomineralizing animal fossils and trace fossils

The Gaojiashan Member of the middle Dengying Formation hosts the Gaojiashan biota, including the earliest biomineralizing animal fossils *Cloudina* and *Sinotubulites* (Hua et al., 2007; Cai et al., 2010; Cai et al., 2011; Cai et al., 2013; Cai et al., 2014; Cai et al., 2015; Cai et al., 2017), other calcareous fossils such as *Pmtolagena* (Cai et al., 2010), nonbiomineralizing tubular fossils such as *Shaanxilithes, Gaojiashania,* and *Conotubus* (Cai et al., 2010), as well as trace fossils made by mobile bilaterian animals (Lin et al., 1986; Zhang, 1986; Ding et al., 1992). *Cloudina* and *Sinotubulites* also extend into the overlying Beiwan Member at the Gaojiashan and nearby Lijiagou sections (Cai et al., 2010). The first appearance datum (FAD) of biomineralizing animals has been regarded as a key datum for the definition of the Terminal Ediacaran Stage (Xiao et al., 2016; Narbonne, 2018).

Chemostratigraphy

The dominance of well-preserved carbonates in the thick Dengying Formation enables global correlations via chemostratigraphy. For example, the carbonate carbon isotope ($\delta^{13}C_{carb}$) profile reveals a positive excursion in the Gaojiashan Member of the Dengying Formation (Cui et al., 2016b), which is likely correlative with a similar magnitude excursion in the basal Khatyspyt Formation in Siberia (Cui et al., 2016a). In addition, large isotopic fluctuations in nitrogen ($\delta^{15}N$), pyrite sulfur ($\delta^{34}S_{pyrite}$), and uranium ($\delta^{238}U$) isotopes have been documented from the Gaojiashan Member of the DYF@GJS (Fig. 13) (Guo et al., 2012; Gamper, 2014; Zhang et al., 2014b; Cui, 2015; Cui et al., 2016b; Zhang et al., 2018). Individually or in unison, these secular stable isotope variations provide potential markers for chemostratigraphic correlations.

Ediacara-type macrofossils

The DYF@GJS has not yet yielded soft-bodied Ediacara-type macrofossils. However, Ediacara-type fossils such as *Pteridinium, Rangea, Charniodiscus, Hiemalora,* and many others have been found in the equivalent Shibantan Member of the Dengying Formation in the Yangtze Gorges area (Sun, 1986; Xiao et al., 2005; Shen et al., 2009; Chen et al., 2014; Mason et al., 2017; Shen et al., 2017).

Age constraints

Based on a U-Pb zircon age of 551.1 ± 0.7 Ma from a volcanic ash at the Doushantuo-Dengying boundary in the Yangtze Gorges area (Condon et al., 2005), and based on a new radiometric constraint of 538.8 Ma from Namibia (Linnemann et al., 2019) for the Ediacaran-Cambrian boundary, the Dengying Formation represents the last 12.3 million years of the Ediacaran Period. In addition, a youngest detrital zircon age of 548 ± 8 Ma (interpreted as the maximum possible depositional age) was reported from the lower Gaojiashan Member of the DYF@GJS (Cui et al., 2016b), which is consistent with the previously published geochronological framework in this region.

Accessibility

The DYF@GJS is located near the Gaojiashan village in the southern Shaanxi Province of South China (Fig. 1), which is easily accessed with field vehicles. From the major city of Hanzhong the drive is ~75 km on the Jingkun Highway (G5) to Hujiaba Town where the vehicles can continue on for an additional 5 km on unpaved road to the base of the section at Huangjia Mountain.

In summary, we regard that the Dengying Formation in South China offers a clear window in which to view the terminal Ediacaran stage. This study builds upon an earlier study (Fig. 13) (Cui, 2015; Cui et al., 2016b) and aims at obtaining high-resolution integrative chemostratigraphic profiles of $\delta^{13}C_{carb}$, $\delta^{18}O_{carb}$, $\delta^{13}C_{org}$, and $\delta^{34}S_{pyrite}$ throughout the formation.

3. Geologic settings

The Dengying Formation at the Gaojiashan section (DYF@GJS) is geographically located near Gaojiashan village in southern Shaanxi Province of South China, and paleogeographically is part of the northwestern Yangtze Block (Fig. 1A–C). It should be noted that the word “Gaojiashan” is used to refer to both the locality (e.g., the Gaojiashan village, the Gaojiashan section, DYF@GJS) and the stratigraphic unit (i.e., the Gaojiashan Member).

Stratigraphically, the Dengying Formation (ca. 551.1–538.8 Ma) is sandwiched between the Ediacaran Doushantuo Formation (ca. 635–551 Ma) and the basal Cambrian Kuanchuanpu Formation (Fig. 1D) (Zhu et al., 2007; Jiang et al., 2011). The Dengying Formation in the studied region is typically subdivided into three members including, in ascending order, the Algal Dolomite (dolostones), the Gaojiashan (limestones and calcareous siltsones), and the Beiwan (dolostones). These three members are generally correlated with the Hamajing, Shibantan, and Baimatuo members, respectively, in the Yangtze Gorges area of South China (Zhou and Xiao, 2007; Zhu et al., 2007; Duda et al., 2015).

The DYF@GJS is at least 631.5 m in thickness, with the Algal Dolostone Member measured at 0–202 m, the Gaojiashan Member at 202–257 m, and the Beiwan Member at 257–631.5 m (Fig. 1D). The basal Algal Dolomite Member and hence the Doushantuo-Dengying boundary are faulted out, indicating that the Dengying Formation is probably thicker than the measured thickness of 631.5 m. The Beiwan Member of the DYF@GJS is overlain by limestones of the Kuanchuanpu Formation and then shales of the Guojiaba Formation. The Kuanchuanpu Formation in southern Shaanxi Province and northeastern Sichuan Province contain basal Cambrian small shelly fossils (SSFs) (Steiner et al., 2004) and the oldest known priapulid-like and kinorhynch-like scalidophoran animals (Liu et al., 2014b; Zhang et al., 2015; Han et al., 2017).

4. Analytical methods

In total 270 rock samples were continuously collected at high stratigraphic resolution from exposed outcrop of the DYF@GJS for systematic sedimentological and chemostratigraphic

investigation. These include 45 samples from the Algal Dolomite Member, 113 samples from the Gaojiashan Member (35 samples collected during the 2009 field season and 78 samples collected during the 2014 field season), and 112 samples from the Beiwan Member. Samples were analyzed for carbonate carbon ($\delta^{13}C_{carb}$) and oxygen ($\delta^{18}O_{carb}$) isotopes, organic carbon isotopes ($\delta^{13}C_{org}$), strontium isotopes ($^{87}Sr/^{86}Sr$), and sulfur isotopes ($\delta^{34}S$) of total sulfur in acidified residues. Sample preparation (including sample cutting, crushing, acidification, and leaching) and geochemical analyses were conducted using standard operation procedures (e.g., Cui et al., 2015; Cui et al., 2018a) in the Department of Geology, University of Maryland.

4.a. Fabric-specific sampling strategy using micro-drills

Many samples in the Dengying Formation comprise multiple generations of diagenetic textures, which likely record isotopic signatures reflecting different sources of alkalinity. To better evaluate the impact of diagenesis on bulk rock carbonate compositions, micro-drilling was guided by petrographic fabrics so that different phases (e.g., cements, intraclasts, micritic matrix, crystal fans, microbial laminae, carbonate veins, nodules, vug fills) were sampled separately on polished slabs using a micro-drilling apparatus, in order to characterize the isotopic signatures of different stages of diagenesis. For the chemostratigraphic purpose, powders for carbonate carbon ($\delta^{13}C_{carb}$), oxygen ($\delta^{18}O_{carb}$), and strontium ($^{87}Sr/^{86}Sr$) isotope analyses were only sampled from the least-altered and least-recrystallized phases in order to minimize the impact of post-depositional process on geochemical signals.

4.b. Carbon and oxygen isotope analysis

Carbonate carbon and oxygen isotopes were measured by continuous flow isotope ratio mass spectrometry in the University of Maryland Paleoclimate Laboratory using a refined method for the analysis and correction of carbon ($\delta^{13}C_{carb}$) and oxygen ($\delta^{18}O_{carb}$) isotopic compositions of 100 μg carbonate samples (Spötl, 2011; Evans et al., 2016). Up to 180 samples loaded into 3.7 mL Labco Exetainer vials and sealed with Labco septa were flushed with 99.999% Helium and manually acidified at 60 °C. The CO_2 analyte gas was isolated via gas chromatography, and water was removed using a Nafion trap prior to admission into an Elementar Isoprime stable isotope mass spectrometer fitted with a continuous flow interface. Data were corrected via automated MATLAB scripting on the Vienna PeeDee Belemnite and LSVEC Lithium Carbonate (VPDB-LSVEC) scale (Coplen et al., 2006) using periodic in-run measurement of international reference carbonate materials and/or in-house standard carbonates, from which empirical corrections for signal amplitude, sequential drift, and one or two-point mean corrections were applied. Precision for both isotopes is routinely better than 0.1‰ (Evans et al., 2016).

4.c. Organic carbon and pyrite sulfur isotope analyses

The organic carbon ($\delta^{13}C_{org}$) and total sulfur ($\delta^{34}S_{TS}$) isotope compositions were measured by combustion of the decalcified residues to CO_2 or SO_2 with a Eurovector elemental analyzer in-line with a second Elementar Isoprime isotope ratio mass spectrometer. Around 15 g of bulk crushed sample was acidified with 3 M HCl to achieve quantitative removal of carbonates. These acidified residues were washed with ultra-pure Milli-Q (18MΩ) water,

centrifuged, decanted, and dried. The residues were packed into folded tin cups for combustion (0.1 to 0.3 mg of V_2O_5 were added to the sulfur samples to aid in combustion), and released CO_2 and SO_2 were used for the analysis of $\delta^{13}C_{org}$ and $\delta^{34}S_{TS}$, respectively. Due to the negligible amount of organic sulfur in the acidified residues, the dominant sulfur species is pyrite. Thus, $\delta^{34}S_{TS}$ values are regarded as a proxy for pyrite sulfur isotope compositions ($\delta^{34}S_{pyrite}$). Uncertainties for carbon and sulfur isotope measurements determined by multiple analyses of standard materials during analytical sessions are better than 0.1‰ and 0.3‰, respectively.

4.d. Strontium isotope analysis

For strontium isotope ($^{87}Sr/^{86}Sr$) analysis, only limestone samples from the Gaojiashan Member were selected for extraction and measurement. Micro-drilled powders (ca. 10 mg) were leached three times in 0.2 M ammonium acetate (pH ~8.2) to remove exchangeable Sr from non-carbonate minerals, and then rinsed three times with Milli-Q water. The leached powder was centrifuged, decanted, and acidified with doubly distilled 0.5 M acetic acid overnight to remove strontium from the carbonate crystal structure. The supernatant was centrifuged to remove insoluble residues, and then decanted, dried, and subsequently dissolved in 200 μl of 3M HNO_3. Strontium separation by cation exchange was carried out using small polyethylene columns containing ~1 cm of Eichrom®Sr specific resin. The column was rinsed with 400 μl of 3 M HNO_3 before the dissolved sample was loaded onto the column. After loading, the sample was sequentially eluted with 200 μl of 3 M HNO_3, 600 μl of 7 M HNO_3, and 100 μl of 3 M HNO_3 to remove the Ca, Rb and REE fractions; the Sr fraction adsorbs strongly to the resin in an acidic environment. The Sr fraction was removed by elution with ~800 μl of 0.05 M HNO_3 and the resultant eluate was collected and dried. Approximately 200–300 ng of the dried sample was transferred onto a degassed and pre-baked (~4.2 A under high vacuum) high purity Re filament with 0.7 μl of Ta_2O_5 activator. Filaments were transferred to a sample carousel, heated under vacuum (~10^{-7} to 10^{-8} atm) to a temperature between 1450 °C and 1650 °C, and analyzed when a stable signal (>1.0 V) was detected on the mass 88 ion beam. The measurements were conducted on a VG Sector 54 thermal ionization mass spectrometer in the TIMS facility of the University of Maryland Geochemistry Laboratories. Approximately 100 $^{87}Sr/^{86}Sr$ ratios were collected for each sample. The data have been corrected for fractionation using the standard value $^{86}Sr/^{88}Sr = 0.1194$. The fraction of ^{87}Sr resulting from *in situ* decay from ^{87}Rb was removed by measurement of rubidium abundance at mass 85. Repeated analyses of the NBS SRM987 standard yielded an average value of $^{87}Sr/^{86}Sr = 0.710245 \pm 0.000011$ (2σ) during the analytical window.

5. Sedimentology of the Dengying Formation

Sedimentological observations of the Dengying Formation at the Gaojiashan section (DYF@GJS) can provide direct paleoenvironmental context for the depositional basin. Various lithofacies with distinct sedimentary textures can be identified in each of the three members of the DYF@GJS, which are summarized below.

5.a. Lithofacies of the Algal Dolomite Member

The Algal Dolomite Member (0–202 m of the DYF@GJS) is dominated by bedded dolostones (including thrombolites) with abundant karstification textures (e.g., botryoidal dolostones, carbonate breccias, authigenic carbonate crystal fans) and other post-depositional alteration (e.g., saddle dolomite cements).

Botryoidal dolostones—Diagnostic karst carbonates are abundant in the outcrop, including void-filling botryoidal dolostone (Fig. 2) and karst breccia (Fig. 3). Botryoidal dolostone typically shows concentric layers around a core in mm to cm scale, suggesting centrifugal precipitation (Fig. 2F, G). Based on their distinct textures, including growth discontinuities and square crystal termination (Fig. 2G–I), it is likely that they were initially aragonite in mineralogy, and were subsequently replaced by calcite and dolomite (e.g., Ginsburg and James, 1976; Aissaoui, 1985; Sandberg, 1985). The occurrences of botryoidal aragonites are typically parallel with the primary bedding.

Carbonate breccias—Closely associated with botryoidal dolostones, carbonate breccia is abundant in the Algal Dolomite Member (Fig. 3A–C). Isopachous cements in botryoidal dolostone were broken into cm-sized breccia and were then cemented after final deposition (Fig. 3). Some primary pores between the carbonate breccias are still not yet fully cemented (Fig. 3B). Petrographic observations reveal that these carbonate breccias are mostly composed of isopachous cements growing on dolomite intraclasts or botryoidal dolostone (Fig. 3D–F).

Authigenic carbonate crystal fans—Distinct authigenic crystal fans in cm size have been found in the Algal Dolomite Member (Fig. 4). These crystal fans were initially misidentified as algal fossils in previous studies (Cao and Zhao, 1978b; Cao and Zhao, 1978a), and then re-interpreted as inorganic carbonate precipitates (Cai et al., 2010). The sharp square crystal terminations and growth discontinuities within the crystal fan (Fig. 4D, E, H, I) suggest that these authigenic cements were initially aragonite in mineralogy (e.g., Mazzullo and Cys, 1979; Mazzullo, 1980; Sandberg, 1985; Corsetti et al., 2004; Pruss et al., 2008; Loyd et al., 2013) and then converted to dolomite (no fizz in acid test) (Aissaoui, 1985; Lin et al., 2015; Peng et al., 2017).

Thrombolites—Thrombolites with distinct clotted texture are abundant in the Algal Dolomite Member (Fig. 4B, Fig. 5A–C). The occurrence of thrombolites in the Dengying Formation (Fang et al., 2003; Li et al., 2013b; Liu et al., 2015; Wang et al., 2016; Chen et al., 2017; Luo et al., 2017; Wen et al., 2017), along with other Ediacaran occurrences in the Ara Group of Oman (Grotzinger et al., 2000; Grotzinger et al., 2005; Grotzinger and Al-Rawahi, 2014) and the Blueflower Formation in the Mackenzie Mountains of Northwestern Canada (Aitken and Narbonne, 1989), suggests that thrombolites were abundant in Ediacaran shallow marine environments.

Saddle dolomite cements—Petrographic observations reveal that many late-stage voidfilling cements are composed of large saddle dolomite crystals, which are characterized by distinct cleavage and sweeping extinction under cross polarized light (Fig. 5D–F). These

saddle dolomite cements are typically interpreted as precipitates from hydrothermal fluids during deep burial (Davies and Smith Jr, 2006; Shi et al., 2013; Liu et al., 2014a; Zhu et al., 2014a), thus should be avoided in chemostratigraphic studies.

5.b. Lithofacies of the Gaojiashan Member

The fossiliferous Gaojiashan Member (202–257 m of the DYF@GJS) is 55 m in thickness, including a siltstone interval in the lower part, repetitious siltstone-mudstone-limestone facies with crinkly and microbially laminated limestone in the middle part, and a coarse sandstone/conglomerate interval at the top (Fig. 6) (Cai et al., 2010; Cui et al., 2016b). Sedimentological observations suggest that the Gaojiashan Member is mainly deposited in a subtidal marine setting between the fair weather and storm wave bases. Limestones with abundant microbial laminae (Fig. 6D–H) and intraclasts in this member (Fig. 6I) suggest sediment reworking by episodic storm events (Cai et al., 2010).

Bedded siltstones or silty limestones (Lower Gaojiashan Member, 202–222 m of the DYF@GJS)—The lower Gaojiashan Member is mainly composed of thinly bedded siltstones or silty limestones without cross bedding textures, suggesting a relatively deep environment. The enigmatic body fossil *Shaanxilithes ningqiangensis* is found in the siltstone facies of this member (Meyer et al., 2012).

Bedded limestones or silty limestones (Middle Gaojiashan Member, 222–254 m of the DYF@GJS)—The middle Gaojiashan Member contains *Conotubus hemiannulatus* and *Gaojiashania cyclus* preserved in thin, normally graded calcisiltite-siltstone beds interpreted as distal event deposits (Cai et al., 2010). Further up section, the first appearance of the biomineralizing animal *Cloudina* occurs in intraclastic limestone facies approximately 40 m above the base of the Gaojiashan Member (Fig. 7A–F) (Hua et al., 2007; Cai et al., 2010). Notably, *Cloudina* fossils at the DYF@GJS are typically associated with microbial laminae (Cai et al., 2014). Similar observations have also been made in the Nama Group of Namibia (Grotzinger and James, 2000; Adams et al., 2004; Grotzinger et al., 2005), the Byng Formation of the Miette Group in British Columbia (Hofmann and Mountjoy, 2001), the Tamengo Formation of the Corumbá Group in Southwest Brazil (Becker-Kerber et al., 2017), and the Itapucumi Group in Paraguay (Warren et al., 2011), where intimate association of *Cloudina* with microbialites have also been reported.

Gypsum (Middle Gaojiashan Member, at 251.5 m of the DYF@GJS)—It is notable that a distinct gypsum (now replaced by calcite) horizon (ca. 2–3 cm in thickness) occurs within the limestone intervals in 5.5 meters below the conglomerate and sandstone interval of the upper Gaojiashan Member (Fig. 7G–I). In this layer, calcite pseudomorphs with distinct gypsum crystal shape suggests the dissolution and replacement of pre-existing gypsum. This gypsum layer, along with sedimentary structures indicative of shallow-water depositional environments, suggests an evaporative environment with high concentrations of seawater sulfate. The presence of gypsum in the DYF@GJS is also consistent with published sedimentological observations in other localities across the Yangtze Block, where evaporites, including halite, gypsum, and anhydrite, have also been widely reported from the Dengying

Formation (Xi, 1987; Siegmund and Erdtmann, 1994; Meng et al., 2011; Lu et al., 2013; Duda et al., 2015; Liu et al., 2015; Luo et al., 2017).

Sandstones and conglomerates (Upper Gaojiashan Member, 254–257 m of the DYF@GJS)—A distinct interval of coarse sandstones and conglomerates occurs in the uppermost Gaojiashan Member, suggesting increasingly shallower depositional environment. This conglomerate and sandstone interval is dominated by pure quartz grains at the DYF@GJS, and shows large-scale cross bedding in the nearby Shiziya section (Cai et al., 2010).

5.c. Lithofacies of the Beiwan Member

The Beiwan Member (257–631.5 m of the DYF@GJS) is dominated by thick-bedded dolostones with void-filling bitumen (Fig. 8). At the outcrop scale, bitumen-rich layers can be parallel to or cross-cut the primary bedding. Petrographic observations in thin sections (Fig. 8) reveal that the pores in the Beiwan dolostones are often surrounded by quartz rims (Fig. 8E, F, H, I, K), suggesting that silicification in low pH conditions may have promoted the dissolution of primary dolostones and contributed to the genesis of secondary porosity. These secondary pores or vugs consequently facilitated oil migration that resulted in the infilling of bitumen in the voids.

5.d. A synthetic depositional model

Based on the above sedimentological observations, the deposition of the DYF@GJS can be divided to multiple stages as described below (Fig. 9).

Stage 1 (Algal Dolomite Member)—The Algal Dolomite Member of the Dengying Formation was rapidly deposited in a relatively warm peritidal environment (Fig. 9A). In light of the repeating occurrences of botryoidal carbonates in parallel with the primary beddings, sea levels were likely low and the carbonate deposits were subject to frequent subaerial exposure, so that syn-depositional or very early post-depositional karstification occurred repeatedly. The void-filling authigenic aragonite cements and crystal fans in this formation may have formed penecontemporaneous with sedimentation when sea level fluctuated and the carbonate sediments were repeated exposed and submerged.

Stage 2 (Lower Gaojiashan Member)—The lower Gaojiashan Member represents deposition below storm wave base, as evidenced by the thinly-bedded siltstone and silty limestones in this unit.

Stage 3 (Middle and upper Gaojiashan Member)—Deposition mostly occurred in an environment above the storm wave base (Cai et al., 2010) (Fig. 9B). Towards the upper Gaojiashan Member, the relative sea level dropped progressively, leading to the deposition of gypsum, carbonate intraclasts, and conglomerate and sandstones.

Stage 4 (Beiwan Member)—The Beiwan Member represents another period of carbonate deposition in peritidal environment with a high sedimentation rate (Fig. 9C).

The overall shallowing trend from the Gaojiashan to the Beiwan Member may have been controlled by regional tectonic uplift (Xue et al., 2001; Wang et al., 2014b; Zhu et al., 2014b; Li et al., 2015; Zhu et al., 2015; Yang et al., 2017). The repeated karstification of the Algal Dolomite Member, on the other hand, may be related to minor sea level fluctuations in a peritidal environment.

6. Geochemical results of the Dengying Formation

6.a. Fabric-specific $\delta^{13}C_{carb}$ and $\delta^{18}O_{carb}$ data

Samples in the dolostone-dominated Algal Dolomite Member and Beiwan Member typically show complex textures, including dolomicrite matrix, large aragonite (now dolomite) crystal fans, and void-filling aragonite (now dolomite) or quartz cements. Fabric-specific geochemical analysis via micro-drilling shows different isotopic signatures among individual phases (Fig. 10). It is notable that the aragonite (now dolomite) crystal fans record the highest $\delta^{18}O_{carb}$ values (−0.9‰ in Fig. 10A and −1.8‰ in Fig. 10C) among the data measured from the microdrilled carbonates. In contrast, late-stage hydrothermal saddle dolomite cements typically show the lowest $\delta^{18}O_{carb}$ values (−10.3‰ in Fig. 10A).

During the field investigation, multiple calcite-filled vugs and veins were found in the limestone intervals of the upper Gaojiashan Member (1–2 meters below the conglomerate/sandstone interval) (Fig. 11A–C). Both the calcite veins and micritic limestone host rock were micro-drilled and analyzed for $\delta^{13}C_{carb}$ and $\delta^{18}O_{carb}$ compositions (Fig. 11D–G). The data show that the $\delta^{13}C_{carb}$ and $\delta^{18}O_{carb}$ values measured from the calcite vugs and veins are consistently lower than those of the limestone host rock.

6.b. Chemostratigraphic profiles of the Dengying Formation

For chemostratigraphic purpose, only data measured from the least-altered micritic carbonate matrix were compiled when constructing the chemostratigraphic profiles (Figs. 12, 13). Carbonate percentage (carbonate wt%) of the DYF@GJS are mostly >90% except for a few siltstone intervals in the Gaojiashan Member (Fig. 12A). The $\delta^{13}C_{carb}$ profile of the DYF@GJS shows a positive excursion (up to +6‰) in the Gaojiashan Member (Fig. 12B, 13B) and two broad positive excursions (up to +4‰) in the Algal Dolomite Member and Beiwan Member, respectively (Figs. 12B,14A). The $\delta^{18}O_{carb}$ data of the DYF@GJS mostly range between −5‰ and 0‰, with the exception of the Gaojiashan Member (down to ca. −8‰, Fig. 13B), the uppermost Beiwan Member, and the Kuanchuanpu Member (Fig. 12B). The organic carbon isotope ($\delta^{13}C_{org}$) data of the DYF@GJS mostly range between −30‰ and −25‰, with more negative values (down to ca. −35‰) in the Gaojiashan and the Kuanchuanpu members (Figs. 12C, 13C). Calculated values of carbon isotope fractionation ($\Delta\delta^{13}C = \delta^{13}C_{carb} - \delta^{13}C_{org}$) between carbonate carbon and organic carbon of the DYF@GJS mostly range between +25‰ and +35‰, with higher values in the Gaojiashan Member and some horizons of the Beiwan Member (Fig. 12D).

Given the potential impact by dolomitization, $^{87}Sr/^{86}Sr$ analysis of the DYF@GJS was only conducted for selected limestone samples from the Gaojiashan Member. Considering that $^{87}Sr/^{86}Sr$ values in carbonates typically increase during burial diagenesis due to the

influence of Rb-rich fluids (Banner, 1995; Jacobsen and Kaufman, 1999), the lowest value likely better represents the primary seawater signals (e.g., Li et al., 2013a). In this study, the lowest $^{87}Sr/^{86}Sr$ value is 0.7084 measured from the limestone sample 09GJS-11 (collected at the stratigraphic height of 246 m of the DYF@GJS, Figs. 12, 13), which is consistent with the published $^{87}Sr/^{86}Sr$ data (ca. 0.7084) measured from the equivalent Shibantan Member in the Yangtze Gorges area (Fig. 14B) (Jiang et al., 2007).

Pyrite sulfur isotope ($\delta^{34}S_{pyrite}$, measured from acidified residues) data of the DYF@GJS show positive values ranging between +10‰ and +40‰ through most of the section, except for two remarkable negative anomalies (down to −30‰) in the siltstone and silty limestone intervals of the middle and lower Gaojiashan Member (Figs. 12E, 13F). The $\delta^{34}S_{cas}$ data of carbonate-associated sulfate (CAS) have only been analyzed for the Gaojiashan Member and have been published previously (Cui et al., 2016b).

7. Discussion

7.a. Timing of the karstification event

The bedded dolostones in the Algal Dolostone Member are mostly composed of dolomicrite matrix and multiple stages of void-filling carbonate cements (Figs. 4, 5). The dolomicrite matrix is very fine grain sized, therefore likely formed as primary precipitates in seawater or during very early diagenesis in a dolomite ocean (Tucker, 1982; Tucker, 1983; Lei and Zhu, 1992; Wang and Xiang, 1999; Corsetti et al., 2006). Notably, the Algal Dolomite Member of the DYF@GJS shows abundant karstification textures. The occurrence of botryoidal dolostones, carbonate breccia, and distinct carbonate crystal fans in this member suggests pervasive karstification followed by void-filling carbonate authigenesis (Figs. 2–4, 10).

Field investigation reveals that the karstification textures in the DYF@GJS are restricted to the lower half of the Algal Dolomite Member, with botryoidal aragonites in parallel with the primary beddings. Based on the stratigraphic relationship, the karstification events of the Algal Dolomite Member should have occurred relatively early, probably penecontemporaneous with the deposition of dolomite sediments in response to sea level fluctuations in a peritidal environment. Sea levels may have been subject to frequent fluctuations so that early karstification could occur repeatedly.

7.b. Origin of the authigenic aragonite cements

Although the authigenic carbonates in the Algal Dolomite Member of the DYF@GJS have already been completely dolomitized, diagnostic textures that suggest an original aragonite mineralogy are retained. Supporting evidence includes large carbonate crystal fans with discontinuities and square termination, botryoidal carbonates and fibrous isopachous cements (Figs. 4, 10), which are all distinct from typical dolomite cements formed during postdepositional diagenesis (Purser et al., 2009; Tucker, 2009).

The origin of the authigenic aragonites in the Algal Dolomite Member remains debated. In geological records, botryoidal aragonites of both marine origin (Ginsburg and James, 1976; Mazzullo and Cys, 1979; Aissaoui, 1985; Jiang et al., 2006a) and non-marine origin (Mazzullo, 1980; Aissaoui, 1985) have been reported. Proposed interpretations for the

Dengying aragonites include primary-syndepositional seafloor precipitates (Zhang, 1980; Cao, 2002; Zhang et al., 2014a; Lin et al., 2015; Peng et al., 2017), authigenic carbonates formed in meteoric waters (Wang et al., 2010; Shi et al., 2011), authigenic carbonates formed in marine environments (Si et al., 2014; Hao et al., 2015; Mou et al., 2015; Tan et al., 2015), and late authigenic carbonates formed during burial diagenesis (Wang et al., 2000).

Based on multiple lines of evidence, an early authigenic marine origin for the Dengying aragonites is preferred in this study. First, the botryoidal aragonites in the Dengying Formation are mostly void-filling, distributed mostly in parallel with the primary sedimentary beddings. Therefore, a syndepositional origin, instead of a syngenetic (in water columns) origin, is more likely.

Second, fabric-specific $\delta^{18}O_{carb}$ values of different carbonate phases reveal that the authigenic aragonite crystal fans show higher $\delta^{18}O_{carb}$ values than the host dolostones (Fig. 10A, C). Considering that meteoric waters typically have much lower $\delta^{18}O$ signals than seawater (Knauth and Kennedy, 2009; Bishop et al., 2014; Oehlert and Swart, 2014), the impact by meteoric waters on these authigenic cements should be minimized. Therefore, an evaporitic marine origin, instead of a karst-related meteoric water origin, is more likely.

Third, published studies show that the late Ediacaran botryoidal aragonites in the Dengying Formation (Zhang et al., 2014a; Lin et al., 2015; Mou et al., 2015; Peng et al., 2017), as well as correlative strata in the Nama Group of Namibia (Grant et al., 1991), typically show dull or non-luminescent color under the cathodoluminescence (CL) light, which is consistent with marine carbonates, instead of late diagenetic carbonates that typically show bright CL colors. In addition, aragonite is unstable in meteoric or late diagenetic fluids, so it is not likely that these aragonite cements formed through late diagenetic processes.

Taken together, based on sedimentological and geochemical results, the botryoidal aragonite textures, aragonite crystal fans, and karstification features in the Algal Dolomite Member of the DYF@GJS were formed during frequent sea level fluctuations and repeated exposure and submergence in a peritidal environment. Thus, although the botryoidal aragonite textures and aragonite crystal fans are technically early post-depositional in origin, they still appear to record seawater signals.

7.c. A high-alkalinity ocean in the terminal Ediacaran Period

If our interpretation of these authigenic aragonite (now dolomite) cements is correct, then the ocean chemistry may have witnessed the occurrence of a high-alkalinity ocean during the terminal Ediacaran Period. The existence of a high-alkalinity ocean at that time is consistent with the sedimentological observations that authigenic aragonites have also been found in the correlative late Ediacaran strata in Namibia (Grant, 1990; Grant et al., 1991; Grotzinger et al., 2000; Wood et al., 2002; Grotzinger et al., 2005; Hall et al., 2013; Penny et al., 2014; Wood, 2016) and the Siberia Platforms (Wood et al., 2017b).

Supporting evidence for a high-alkalinity ocean in the terminal Ediacaran Period also comes from the strontium concentration data. Published geochemical data show elevated concentrations of strontium in the carbonates of the Dengying Formation in South China

(Fig. 13G) (Sawaki et al., 2010; Cui et al., 2016b) and the Nama Group of Namibia (Grant et al., 1991; Ries et al., 2009). Considering that strontium has a crystal ionic radius larger than that of Ca^{2+} and thus prefers the more open octahedral crystal structure of aragonite over the smaller hexagonal structure of calcite (Wray and Daniels, 1957; Lorens, 1981), the precipitation of aragonites in a high-alkalinity ocean during deposition could account for the enrichment of strontium concentrations in marine carbonates during the late Ediacaran Period.

Taken together, it is likely that a high-alkalinity ocean occurred in the late Ediacaran Period. This inferred high-alkalinity ocean was evidenced by the authigenic aragonites in the Algal Dolomite Member and high Sr concentrations in the Gaojiashan Member of the Dengying Formation.

7.d. Evaluating the impact of authigenesis

Given the significant heterogeneity of carbonates in the studied samples, fabric-specific $\delta^{13}C_{carb}$ and $\delta^{18}O_{carb}$ analysis of different phases and textures the DYF@GJS was adopted as the sampling strategy. Guided by detailed sedimentological observations, we evaluated the impact of authigenesis for each of the three members.

Authigenesis of the Algal Dolomite Member—Authigenic aragonite (now dolomite) crystal fans from the Algal Dolomite Member have been investigated for $\delta^{13}C_{carb}$ and $\delta^{18}O_{carb}$ values by micro-drilling analysis (Fig. 1). The $\delta^{18}O_{carb}$ values of the dolomitized crystal fans (−0.9‰ in Fig. 10A and −1.8‰ in Fig. 10C) are notably enriched in ^{18}O compared with other carbonate phases, suggesting high-alkalinity evaporative conditions during precipitation (Ufnar et al., 2008; Gomez et al., 2014; Guo and Chafetz, 2014; Horton et al., 2015; Leleu et al., 2016). On the contrary, isotope data of the late carbonate cements, particularly the hydrothermal saddle dolomite, show much lower $\delta^{18}O_{carb}$ values (ca. −10‰) than early crystal fans and dolomitic matrix, which is consistent with a high-temperature origin during deep burial. Similar observations of hydrothermal dolomite in the Dengying Formation in the Sichuan Basin (Shi et al., 2013; Liu et al., 2014a; Jiang et al., 2016) suggest that the occurrence of saddle dolomite in the Dengying Formation may result from a basin-scale geothermal event during deep burial.

Authigenesis of the Gaojiashan Member—Multiple calcite-filled vugs and veins were found in the limestone intervals of the upper Gaojiashan Member (1–2 meters below the conglomerate/sandstone interval) (Fig. 11A-C). We micro-drilled and analyzed the $\delta^{13}C_{carb}$ and $\delta^{18}O_{carb}$ values of both the calcite veins and micritic limestone phases in order to evaluate the impact of diagenesis (Fig. 11D-G). The $\delta^{13}C_{carb}$ and $\delta^{18}O_{carb}$ values of the calcite veins show more negative values compared with the host limestone rocks (Fig. 11). Two interpretations could possibly explain this observation: (1) These calcite veins may be early authigenic carbonates formed by microbial sulfate reduction (MSR) in pore waters (e.g., Campbell et al., 2002; Jiang et al., 2003; Jiang et al., 2006a; Jiang et al., 2006b; Schrag et al., 2013; Zhou et al., 2016; Cui et al., 2017a), or (2) these calcite veins may result from intrusions of late diagenetic fluids (e.g., Bristow et al., 2011; Lin et al., 2011). Based on the sharp contact between these white calcite phases and the host carbonates, which sometimes

cut across the primary sedimentary beddings, a late diagenetic origin for these calcite phases is preferred in this study.

Recently, largely based on a newly discovered $\delta^{13}C_{carb}$ negative excursion in the upper Gaojiashan Member, Gamper et al. (2015) placed the Ediacaran-Cambrian boundary in the middle Dengying Formation. However, it should be noted that this $\delta^{13}C_{carb}$ negative excursion occurs in the conglomerate/sandstone interval of the uppermost Gaojiashan Member, which more likely reflects late diagenetic signals instead of primary seawater signals. Therefore, the Gamper et al.'s (2015) placement of the Ediacaran-Cambrian boundary should be treated with caution. Our observation of late diagenetic calcite veins with negative $\delta^{13}C_{carb}$ values around this interval casts doubt on the fidelity of the proposed $\delta^{13}C_{carb}$ negative excursion and its relationship with the Ediacaran-Cambrian boundary.

Authigenesis of the Beiwan Member—Bitumen-bearing dolostones in the Beiwan Member have also been tested to evaluate the impact of bitumen on the $\delta^{13}C_{carb}$ and $\delta^{18}O_{carb}$ values. Potential oxidation of the bitumen may have caused a significant decrease in $\delta^{13}C_{carb}$ values (e.g., Bristow et al., 2011). However, no strongly negative $\delta^{13}C_{carb}$ values have been found in the bitumen-bearing samples (Fig. 8L), suggesting little impact of bitumen on the $\delta^{13}C_{carb}$ compositions. That being said, it is notable that the $\delta^{13}C_{org}$ data in the Beiwan Member show large variations (Fig. 12C), which may be caused by the influence of bitumen in the dolostone samples.

In summary, the texture-specific micro-drilling method employed in this study demonstrates that coupled petrographic and isotope analysis is an informative tool for the evaluation of diagenetic influences in chemostratigraphic studies. Late diagenetic signatures should be identified and treated with caution in paleoenvironmental interpretations.

7.e. Biogeochemical carbon cycles

The chemostratigraphic $\delta^{13}C_{carb}$ profile of the DYF@GJS show a positive excursion up to +6‰ in the Gaojiashan Member (Figs. 1D, 12B, 13B). Comparisons of the $\delta^{13}C_{carb}$ profile with other Dengying or equivalent sections at regional and global scales show both similarities and differences (Fig. 14). In the Yangtze Block, similar $\delta^{13}C_{carb}$ positive excursions have also been reported from correlative Ediacaran sections at Shipai (Jiang et al., 2007), Jiulongwan (Wang et al., 2014a), Lianghekou (Chen et al., 2015), Lianghong (Wang et al., 2012), and Huajipo (Zhang et al., 2004) (Fig. 14). The difference in the chemostratigraphic $\delta^{13}C_{carb}$ profiles of these sections may result from difference in local redox conditions, sedimentation rates, stratigraphic hiatus, or sampling resolutions. Regardless, most of the sections show a $\delta^{13}C_{carb}$ excursion up to +6‰.

Viewed at a global scale, the finding of a $\delta^{13}C_{carb}$ excursion up to +6‰ in the Dengying Formation is also consistent with published chemostratigraphic profiles of the roughly correlative late Ediacaran strata in Namibia (Saylor et al., 1998; Wood et al., 2015; Tostevin et al., 2017) and Arctic Siberia (Knoll et al., 1995; Pelechaty et al., 1996b; Cui et al., 2016a; Vishnevskaya et al., 2017) where $\delta^{13}C_{carb}$ positive excursions with similar magnitude (up to +6‰) have also been reported.

Two hypotheses may be able to explain this $\delta^{13}C_{carb}$ positive excursions. Frist, canonical models of the global carbon cycle suggests that $\delta^{13}C_{carb}$ positive anomalies likely result from an enhanced organic carbon burial rate because organic carbon is strongly enriched in ^{12}C (Broecker, 1970; Hayes et al., 1999). Alternatively, a $\delta^{13}C_{carb}$ positive excursion can also result from the mixing of high-$\delta^{13}C_{carb}$ authigenic carbonates during early diagenesis. This is possible if residual carbon after fermentation (methanogenesis) led to the formation of authigenic carbonates (Claypool and Kaplan, 1974; Irwin et al., 1977; Talbot and Kelts, 1986; Meister et al., 2007; Wehrmann et al., 2011; Birgel et al., 2015; Pierre et al., 2016). Such processes may have been particularly prevalent in the Precambrian ocean where the seawater was mostly anoxic and therefore may promote authigenic carbonate precipitation on the seafloor (Higgins et al., 2009; Schrag et al., 2013).

Based on multiple lines of evidence, we prefer the former hypothesis (i.e., enhanced organic carbon burial) for this $\delta^{13}C_{carb}$ positive excursion. Frist, no extremely high or low $\delta^{13}C_{carb}$ signals that are indicative of the existence of methane have been found based on our detailed geochemical analysis of micro-drilled samples. Therefore, there is no supporting evidence for the occurrence of methane generation or oxidation in the DYF@GJS. Second, the presence of a gypsum layer near the height of the $\delta^{13}C_{carb}$ positive excursion at the middle Gaojiashan Member of the DYF@GJS suggests that the sulfate concentration was high during the $\delta^{13}C_{carb}$ excursion. Considering that methanogens are typically outcompeted for substrates (e.g. lactate and acetate) by sulfate reducers in sulfate-rich environments (Jørgensen and Kasten, 2006), methanogenesis would not have played a considerable role in generating this $\delta^{13}C_{carb}$ positive excursion. Third, the recent investigations by N and U isotopes (Fig. 13) suggest that extensive oceanic anoxia occurred during the late Ediacaran (Wei et al., 2018; Zhang et al., 2018). This oceanic anoxia event may have promoted organic carbon burial and led to the $\delta^{13}C_{carb}$ positive excursion.

In summary, a $\delta^{13}C_{carb}$ excursion up to +6‰ has been found in the Dengying Formation and many other correlative late Ediacaran sections. Based on multiple lines of evidence, we regard that enhanced organic carbon burial may have caused this excursion.

7.f. Biogeochemical sulfur cycles

Sulfur isotope chemostratigraphy of the DYF@GJS shows overall positive $\delta^{34}S_{pyrite}$ values ranging between +20‰ and +30‰ through most of the section, except for two episodes of anomalous negative excursions down to ca. −30‰ in the lower and middle Gaojiashan Member (Figs. 12E, 13F). The occurrence of highly positive $\delta^{34}S_{pyrite}$ values in the late Ediacaran strata has also been reported from the roughly equivalent strata in Oman (Fike and Grotzinger, 2008), Namibia (Ries et al., 2009; Tostevin et al., 2017), Arctic Siberia (Cui et al., 2016a), and Newfoundland (Canfield et al., 2007; Hantsoo et al., 2018), suggesting a global phenomenon. The origin of the low $\delta^{34}S_{pyrite}$ signals in the Gaojiashan Member has been fully discussed in our earlier paper (Cui et al., 2016b), we will mainly focus on the overall high $\delta^{34}S_{pyrite}$ signals below.

Four hypotheses can be proposed to explain the overall positive $\delta^{34}S_{pyrite}$ signals in the studied section. They are discussed below.

First, thermochemical sulfate reduction (TSR)—The high $\delta^{34}S_{pyrite}$ values may result from Rayleigh fractionations during TSR of hydrothermal fluids in post-depositional processes. Such scenario has recently been proposed for the Cryogenian Datangpo Formation, where extremely high $\delta^{34}S_{pyrite}$ values (up to +70‰) have been found (Cui et al., 2017b; Cui et al., 2018b; Cui et al., 2018c). However, our field observation revealed no clear evidence for a significant impact by hydrothermal fluids. Moreover, assuming a seawater $\delta^{34}S_{sulfate}$ value of +40‰ for the late Ediacaran ocean based on gypsum or carbonate-associated sulfate (CAS) analyses (Fike and Grotzinger, 2008; Bergmann, 2013; Cui et al., 2016b), these $\delta^{34}S_{pyrite}$ values, though positive, still can be explained by microbial sulfate reduction with normal (rather than reversed) fractionations (i.e., $\Delta^{34}S_{sulfate\text{-}pyrite} = \delta^{34}S_{sulfate} - \delta^{34}S_{pyrite} > 0$). Therefore, a TSR origin for the overall high $\delta^{34}S_{pyrite}$ values in the DYF@GJS is not preferred in this study.

Second, low sulfate concentrations of seawater—The positive $\delta^{34}S_{pyrite}$ values may reflect limited S isotope fractionation in seawaters with very low concentrations of sulfate (Habicht et al., 2002; Loyd et al., 2012). However, given the presence of gypsum in the Dengying Formation across the Yangtze platform and the overall shallow and evaporative environments inferred from the lithofacies, seawater sulfate concentration should not be a limiting factor for microbial sulfate reduction. Therefore, this hypothesis is not favored here.

Third, higher proportions of pyrite burial—The overall positive $\delta^{34}S_{pyrite}$ signals in the late Ediacaran Period may be caused by enhanced rates of pyrite burial. This scenario has been proposed based on an earlier study of the late Ediacaran strata in Oman (Fike and Grotzinger, 2008). More recent studies of the Dengying Formation have shown notably high $\delta^{15}N$ signals and low $\delta^{238}U$ signals (Fig. 13) indicative of a significant ocean anoxic event with enhanced denitrification and U removal from the ocean into the sediments (Gamper, 2014; Wei et al., 2018; Zhang et al., 2018). This inferred ocean anoxic event at that time may have promoted organic carbon and pyrite burial, leading to the high $\delta^{34}S_{pyrite}$ signals.

Fourth, high sedimentation rates—It is also possible that enhanced sedimentation rates may have contributed to the overall positive $\delta^{34}S_{pyrite}$ signals in the studied section. It has been found that higher sedimentation rate could cause higher $\delta^{34}S_{pyrite}$ in marine sediments (Pasquier et al., 2017; Liu et al., 2019). Although karstification may have eroded the Algal Dolomite Member, compared with the well-studied Doushantuo Formation in the Yangtze Block (Zhou and Xiao, 2007; Zhu et al., 2007; McFadden et al., 2008; Jiang et al., 2011; Zhu et al., 2013; Cui et al., 2015), the Dengying Formation is remarkably thick (Fig. 15). The general thickness of the Doushantuo Formation (ca. 635.2–551.1 Ma) is <300 m in thickness for over 80 million years (Condon et al., 2005; Zhou and Xiao, 2007; Zhu et al., 2007), while the studied DYF@GJS (ca. 551.1–538.8 Ma) is >630 m in thickness for only ~12.3 million years (Fig. 15). Given the exceptionally high sedimentation rate of the Dengying Formation compared with the underlain Doushantuo Formation, it is likely that high sedimentation rate may have also played a role in generating the positive $\delta^{34}S_{pyrite}$ signals.

Taken together, based on multiple lines of sedimentological and geochemical evidence, we regard that enhanced rates pyrite burial may be the main cause of the overall positive $\delta^{34}S_{pyrite}$ values. High sedimentation rates may have also contributed to the high $\delta^{34}Sp_{yrite}$ values, but more information is needed to specifically test this hypothesis.

7.g. Implications on early metazoan evolution

The contrasting thickness between the Dengying Formation and the underlying Doushantuo Formation can provide useful insights into the changing environment. This sharp contrast suggests that the depositional environment during the late Ediacaran Period has been subject to significant change, which is possibly characterized by overall shallower water depth, higher alkalinity, and higher accommodation space. Such conditions are suitable for continuous production and accumulation of marine carbonates.

Sedimentological observations suggest that the karstification events of shallow carbonate platforms may be widespread in the late Ediacaran Period. Notably, similar karstification textures of carbonate breccia, aragonite crystal fans and botryoidal aragonites have also been found from other correlative sections, including the other Dengying sections in South China (Zhang, 1980; Cao and Xue, 1983; Siegmund and Erdtmann, 1994; Xiang et al., 2001; Wang et al., 2010; Shi et al., 2011; Liu et al., 2012; Wang et al., 2012; Mo et al., 2013; Zhang et al., 2014a; Lin et al., 2015; Mou et al., 2015; Lian et al., 2016; Lian et al., 2017), the Qigebulake Formation in the Tarim basin in Northwestern China (Qian et al., 2017), the Buah Formation in Oman (Gorin et al., 1982; Cozzi and Al-Siyabi, 2004; Bergmann, 2013), the K3 and K4 units of the Katakturuk Dolomite succession in Arctic Alaska (Macdonald et al., 2009), and the Turkut Formation in the Siberia Platform (Knoll et al., 1995; Pelechaty et al., 1996a; Nagovitsin et al., 2015; Rogov et al., 2015; Cui et al., 2016a). These observations suggest widespread karstification of shallow carbonate platforms at a global scale.

The overall shallow marine environment may be caused by regional tectonic uplift in the depositional basin (Xue et al., 2001; Wang et al., 2014b; Zhu et al., 2014b; Li et al., 2015; Zhu et al., 2015; Yang et al., 2017). The extensive karstification of shallow carbonate platforms during the late Ediacaran Period was probably triggered by fluctuations of relative sea level at that time. This scenario is in agreement with an overall increase in seawater $^{87}Sr/^{86}Sr$ and decrease in seawater Nd isotopes through the Proterozoic-Phanerozoic transition (Halverson et al., 2007; Halverson et al., 2010; Peters and Gaines, 2012; Cox et al., 2016). The breakup of the Rodinia supercontinent and assembly of the Gondwana supercontinent may have profoundly reshaped the Earth surface's lithosphere and hydrosphere and triggered the evolutionary innovation of the biosphere.

Although the precise mechanism is still unclear, the geochemistry of late Ediacaran oceans may have played a role in early animal biomineralization. Considering that the skeletons of the late Ediacaran biomineralizing animal are mostly composed of aragonite or high-Mg calcite (Grant, 1990; Fedorov and Zhuravlev, 1993; Grotzinger et al., 2000; Zhuravlev and Wood, 2008; Zhuravlev et al., 2012), the occurrence of a high-alkalinity ocean — evidence by authigenic aragonite cements — may have influenced the composition of the earliest bio-minerals of early animals. It is likely that the high concentration of alkalinity and nutrient influx in the ocean may have caused the supersaturation of marine carbonates and facilitated

the early animal biomineralization in this critical period (Zhuravlev and Wood, 2008; Peters and Gaines, 2012; Cui et al., 2016b; Wood et al., 2017a).

8. Conclusions

Integrated sedimentological and chemostratigraphic study was conducted for the late Ediacaran Dengying Formation at the Gaojiashan section (DYF@GJS), Ningqiang County of southern Shaanxi Province, South China. Multiple types of lithofacies and diagenesis have been identified and summarized based on detailed field observations, petrographic studies, and isotope measurements of micro-drilled spots.

1. (1) The DYF@GJS was deposited in a largely shallow marine platform with dynamic sea level changes and overall high accommodation space, though the lower Gaojiashan Member may represent a temporary deeper and more anoxic environment. Sedimentological evidence suggests that extensive karstification of shallow marine platforms occurred soon after the deposition of the lower part of the Algal Dolomite Member.
2. (2) We propose that the finding of authigenic aragonites in the Algal Dolostone Member may have significant implications on the Ediacaran ocean chemistry. The micro-drilling $\delta^{18}O_{carb}$ data of the authigenic aragonites (now dolomites) suggest that meteoric waters have little impact on the genesis of these authigenic aragonites. Instead, the Dengying authigenic aragonites may form in marine environments during repeated sea level fluctuations in a peritidal environment, which resulted in karstification features formed during subaerial exposure, followed by void-filling aragonite botryoids formed during submergence. These Dengying authigenic aragonites reflect the existence of a high-alkalinity ocean at that time.
3. (3) Geochemical analysis of micro-drilled samples reveals different compositions among depositional, early authigenic, and late diagenetic components. The post-depositional phases should be excluded when conducting chemostratigraphic profiles.
4. (4) Chemostratigraphic data show a $\delta^{13}C_{carb}$ positive excursion (up to +6‰) in the Gaojiashan Member and overall positive $\delta^{34}S_{pyrite}$ values in most of the Dengying Formation. Based on multiple lines of sedimentological and geochemical evidence, enhanced burial of organic matter and pyrite in shallower environments is proposed for the studied basin. High concentrations of seawater alkalinity and nutrient may have facilitated the evolutionary innovation of early metazoan biomineralization.

Supplementary Material

Refer to Web version on PubMed Central for supplementary material.

Acknowledgment

This study was started when the first author HC was a Ph.D. graduate student at the University of Maryland. It was progressively improved during HC's first postdoc at the NASA Astrobiology Institute at the University of Wisconsin-Madison and HC's second postdoc at the Free University of Brussels (Vrije Universiteit Brussel, VUB), Belgium. HC would like to thank the UMD Geology Department, the NASA Astrobiology Institute at UW-Madison, the ET-HOME (Evolution and Tracers of the Habitability of Mars and Earth) Astrobiology Research Consortium in Belgium, and the AMGC-VUB for support.

The authors would like to thank Mike Evans, Yongbo Peng, Zhengting Wang, Brittney Gaeta, and Elizabeth Lee for their assistance in the UMD Paleoclimate Laboratory; Xiao Min from Northwest University and Fazhi Li from the Gaojiashan Village for their assistance in field work. The authors would also like to thank three anonymous reviewers, whose constructive comments have significantly improved the clarity of this manuscript.

This research is funded by the American Association of Petroleum Geologists (AAPG) Grants-In-Aid Program Marilyn Atwater Memorial Grant to HC, the Explorers Club Washington Group grant to HC, the NASA Exobiology grant (NNX12AR91G to AJK and 80NSSC18K1086 to SX), the NSF Sedimentary Geology and Paleontology grant (EAR0844270 to AJK; EAR1528553 to SX), and the Young Scientists Fund of Shaanxi Province (No. 2015KJXX-26) to YC.

References

Adams EW, Schröder S, Grotzinger JP and Mccormick DS (2004) Digital reconstruction and stratigraphic evolution of a microbial-dominated, isolated carbonate platform (terminal Proterozoic, Nama Group, Namibia). Journal of Sedimentary Research 74, 479–497. 10.1306/122903740479

Aissaoui DM (1985) Botryoidal aragonite and its diagenesis. Sedimentology 32, 345–361. 10.1111/j.1365-3091.1985.tb00516.x

Aitken JD and Narbonne GM (1989) Two occurrences of Precambrian thrombolites from the Mackenzie Mountains, northwestern Canada. Palaios 4, 384–388. 10.2307/3514563

Banner JL (1995) Application of the trace element and isotope geochemistry of strontium to studies of carbonate diagenesis. Sedimentology 42, 805–824. 10.1111/j.1365-3091.1995.tb00410.x

Becker-Kerber B, Pacheco MLaF, Rudnitzki ID, Galante D, Rodrigues F and De Moraes Leme J (2017) Ecological interactions in *Cloudina* from the Ediacaran of Brazil: implications for the rise of animal biomineralization. Scientific reports 7, 5482 10.1038/s41598-017-05753-8 [PubMed: 28710440]

Bergmann KD, (2013) Constraints on the Carbon Cycle and Climate during the Early Evolution of Animals. Ph.D. Dissertation Thesis, California Institute of Technology, Pasadena, California, 398 pp. http://resolver.caltech.edu/CaltechTHESIS:06102013-045943358

Birgel D, Meister P, Lundberg R, Horath TD, Bontognali TRR, Bahniuk AM, De Rezende CE, Vasconcelos C and Mckenzie JA (2015) Methanogenesis produces strong 13C enrichment in stromatolites of Lagoa Salgada, Brazil: a modern analogue for Palaeo-/Neoproterozoic stromatolites? Geobiology 13, 245–266. 10.1111/gbi.12130 [PubMed: 25773379]

Bishop JW, Osleger DA, Montañez IP and Sumner DY (2014) Meteoric diagenesis and fluid-rock interaction in the Middle Permian Capitan backreef: Yates Formation, Slaughter Canyon, New Mexico. AAPG Bulletin 98, 1495–1519. 10.1306/05201311158

Bristow TF, Bonifacie M, Derkowski A, Eiler JM and Grotzinger JP (2011) A hydrothermal origin for isotopically anomalous cap dolostone cements from south China. Nature 474, 68–71. 10.1038/nature10096 [PubMed: 21613997]

Broecker WS (1970) A boundary condition on the evolution of atmospheric oxygen. Journal of Geophysical Research 75, 3553–3557. 10.1029/JC075i018p03553

Cai Y, Hua H, Xiao S, Schiffbauer JD and Li P (2010) Biostratinomy of the late Ediacaran pyritized Gaojiashan Lagerstätte from southern Shaanxi, South China: Importance of event deposits. Palaios 25, 487–506. 10.2110/palo.2009.p09-133r

Cai Y, Schiffbauer JD, Hua H and Xiao S (2011) Morphology and paleoecology of the late Ediacaran tubular fossil Conotubus hemiannulatus from the Gaojiashan Lagerstätte of southern Shaanxi Province, South China. Precambrian Research 191,46–57. 10.1016/j.precamres.2011.09.002

Cai Y, Hua H and Zhang X (2013) Tube construction and life mode of the late Ediacaran tubular fossil Gaojiashania cyclus from the Gaojiashan Lagerstätte. Precambrian Research 224, 255–267. 10.1016/j.precamres.2012.09.022

Cai Y, Hua H, Schiffbauer JD, Sun B and Yuan X (2014) Tube growth patterns and microbial mat-related lifestyles in the Ediacaran fossil Cloudina, Gaojiashan Lagerstätte, South China. Gondwana Research 25, 1008–1018. 10.1016/j.gr.2012.12.027

Cai Y, Xiao S, Hua H and Yuan X (2015) New material of the biomineralizing tubular fossil Sinotubulites from the late Ediacaran Dengying Formation, South China. Precambrian Research 261, 12–24. 10.1016/j.precamres.2015.02.002

Cai Y, Cortijo I, Schiffbauer JD and Hua H (2017) Taxonomy of the late Ediacaran index fossil *Cloudina* and a new similar taxon from South China. Precambrian Research 298, 146–156. 10.1016/j.precamres.2017.05.016

Campbell K, Farmer J and Des Marais D (2002) Ancient hydrocarbon seeps from the Mesozoic convergent margin of California: carbonate geochemistry, fluids and palaeoenvironments. Geofluids 2, 63–94. 10.1046/j.1468-8123.2002.00022.x

Canfield DE, Poulton SW and Narbonne GM (2007) Late-Neoproterozoic deep-ocean oxygenation and the rise of animal life. Science 315, 92–95. 10.1126/science.1135013 [PubMed: 17158290]

Cao R and Zhao W (1978a) Manicosiphoniaceae, a new family of fossil algae from the Sinian System of SW China with reference to its systematic position. Acta Palaeontologica Sinica 17, 29–40 (in Chinese with English abstract)

Cao R and Zhao W (1978b) The algal flora of the Tongying Formation (upper Sinian System) in southwestern China: Memoir Nanjing Institute of Geology and Palaeontology. Academia Sinica 10, 1–28 (in Chinese with English abstract)

Cao R and Xue Y (1983) Vadose pisolites of the Tongying Formation (Upper Sinian System) in southwest China In Coated Grains (ed Peryt TM). pp. 538–547. Berlin: Springer Berlin Heidelberg 10.1007/978-3-642-68869-044

Cao R (2002) The sedimentary environment of grapestone in Dengying formation of Sinian system in Sichuan and Yunnan. Yunnan Geology 21, 208–213 (in Chinese with English abstract)

Chen Y, Chu X, Zhang X and Zhai M (2015) Carbon isotopes, sulfur isotopes, and trace elements of the dolomites from the Dengying Formation in Zhenba area, southern Shaanxi: Implications for shallow water redox conditions during the terminal Ediacaran. Science China: Earth Sciences 58, 1107–1122. 10.1007/s11430-015-5071-0

Chen Y, Shen A, Pan L, Zhang J and Wang X (2017) Origin and distribution of microbial dolomite reservoirs: A case study of 4th Member of Sinian Dengying Formation in the Sichuan Basin, SW China. Petroleum Exploration and Development 5, 704–715 (in Chinese with English abstract). 10.11698/PED.2017.05.00

Chen Z, Zhou C, Xiao S, Wang W, Guan C, Hua H and Yuan X (2014) New Ediacara fossils preserved in marine limestone and their ecological implications. Scientific reports 4, 4180 10.1038/srep04180 [PubMed: 24566959]

Chen Z, Chen X, Zhou C, Yuan X and Xiao S (2018) Late Ediacaran trackways produced by bilaterian animals with paired appendages. Science Advances 4, eaao6691 10.1126/sciadv.aao6691 [PubMed: 29881773]

Claypool GE and Kaplan I (1974) The Origin and Distribution of Methane in Marine Sediments In Natural Gases in Marine Sediments (ed I.R. K). pp. 99–139. Boston, MA: Springer 10.1007/978-1-4684-2757-88

Condon D, Zhu M, Bowring S, Wang W, Yang A and Jin Y (2005) U-Pb ages from the Neoproterozoic Doushantuo Formation, China. Science 308, 95–98. 10.1126/science.1107765 [PubMed: 15731406]

Coplen TB, Brand WA, Gehre M, Gröning M, Meijer HaJ, Toman B and Verkouteren RM (2006) New Guidelines for δ13C Measurements. Analytical Chemistry 78, 2439–2441. 10.1021/ac052027c [PubMed: 16579631]

Corsetti FA, Lorentz NJ and Pruss SB (2004) Formerly-aragonite seafloor fans from Neoproterozoic strata, Death Valley and southeastern Idaho, United States: Implications for “cap carbonate” formation and Snowball Earth In The Extreme Proterozoic: Geology, Geochemistry, and Climate

eds Jenkins GS, McMenamin MAS, McKay CP and Sohl L). pp. 33–44. American Geophysical Union 10.1029/146gm04

Corsetti FA, Kidder DL and Marenco PJ (2006) Trends in oolite dolomitization across the Neoproterozoic-Cambrian boundary: A case study from Death Valley, California. Sedimentary Geology 191, 135–150. 10.1016/j.sedgeo.2006.03.021

Cox GM, Halverson GP, Stevenson RK, Vokaty M, Poirier A, Kunzmann M, Li Z-X, Denyszyn SW, Strauss JV and Macdonald FA (2016) Continental flood basalt weathering as a trigger for Neoproterozoic Snowball Earth. Earth and Planetary Science Letters 446, 89–99. 10.1016/j.epsl.2016.04.016

Cozzi A and Al-Siyabi HA (2004) Sedimentology and play potential of the late Neoproterozoic Buah Carbonates of Oman. GeoArabia 9, 11–36

Cui H, (2015) Authigenesis, Biomineralization, and Carbon-Sulfur Cycling in the Ediacaran Ocean. Ph.D. Dissertation Thesis, University of Maryland, College Park, Maryland, USA, 181 pp. http://hdl.handle.net/1903/17317

Cui H, Kaufman AJ, Xiao S, Zhu M, Zhou C and Liu X-M (2015) Redox architecture of an Ediacaran ocean margin: Integrated chemostratigraphic (δ13C- δ34S-87Sr/86Sr-Ce/Ce*) correlation of the Doushantuo Formation, South China. Chemical Geology 405, 48–62. 10.1016/j.chemgeo.2015.04.009

Cui H, Grazhdankin DV, Xiao S, Peek S, Rogov VI, Bykova NV, Sievers NE, Liu X-M and Kaufman AJ (2016a) Redox-dependent distribution of early macro-organisms: Evidence from the terminal Ediacaran Khatyspyt Formation in Arctic Siberia. Palaeogeography, Palaeoclimatology, Palaeoecology 461, 122–139. 10.1016/j.palaeo.2016.08.015

Cui H, Kaufman AJ, Xiao S, Peek S, Cao H, Min X, Cai Y, Siegel Z, Liu XM, Peng Y, Schiffbauer JD and Martin AJ (2016b) Environmental context for the terminal Ediacaran biomineralization of animals. Geobiology 14, 344–363. 10.1111/gbi.12178 [PubMed: 27038407]

Cui H, Kaufman AJ, Xiao S, Zhou C and Liu X-M (2017a) Was the Ediacaran Shuram Excursion a globally synchronized early diagenetic event? Insights from methane-derived authigenic carbonates in the uppermost Doushantuo Formation, South China. Chemical Geology 450, 59–80. 10.1016/j.chemgeo.2016.12.010

Cui H, Kitajima K, J. Spicuzza M, Fournelle J, Ishida A, Denny A, Zhang F and Valley J (2017b) Primary or Secondary? Testing the Neoproterozoic Superheavy Pyrite by SIMS. Geological Society of America Abstracts with Programs. Vol. 49, No. 6, Seattle, Washington, USA. 10.1130/abs/2017AM-300028

Cui H, Kaufman AJ, Peng Y, Liu X-M, Plummer RE and Lee EI (2018a) The Neoproterozoic Hüttenberg $\delta^{13}C$ anomaly: Genesis and global implications. Precambrian Research 313, 242–262. 10.1016/j.precamres.2018.05.024

Cui H, Kitajima K, Spicuzza MJ, Fournelle JH, Denny A, Ishida A, Zhang F and Valley JW (2018b) Questioning the biogenicity of Neoproterozoic superheavy pyrite by SIMS. American Mineralogist 103, 1362–1400. 10.2138/am-2018-6489

Cui H, Kitajima K, Spicuzza MJ, Fournelle JH, Denny A, Ishida A, Zhang F and Valley JW (2018c) Questioning the Biogenicity of Neoproterozoic Superheavy Pyrite. Goldschmidt2018 Abstract, Boston, Massachusetts, USA. https://goldschmidt.info/2018/abstracts/abstractView?id=2018001760

Davies GR and Smith LB Jr (2006) Structurally controlled hydrothermal dolomite reservoir facies: An overview. AAPG Bulletin 90, 1641–1690. 10.1306/05220605164

Ding L, Zhang L, Li Y and Dong J (1992) The Study of the Late Sinian-Early Cambrian Biotas from the Northern Margin of the Yangtze Platform. Scientific and Technical Documents Publishing House, Beijing, 135 pp.

Duda J-P, Zhu M and Reitner J (2015) Depositional dynamics of a bituminous carbonate facies in a tectonically induced intra-platform basin: the Shibantan Member (Dengying Formation, Ediacaran Period). Carbonates and Evaporites 31, 87–99. 10.1007/s13146-015-0243-8

Evans M, Selmer K, Breeden B, Lopatka A and Plummer R (2016) Correction algorithm for on-line continuous flow $\delta^{13}C$ and $\delta^{18}O$ carbonate and cellulose stable isotope analyses. Geochemistry, Geophysics, Geosystems 17, 3580–3588. 10.1002/2016GC006469

Fang S, Hou F and Dong Z (2003) Non-stromatoltite ecologic system cyanobacteria dolostone in Dengying Formation of Upper-Sinian. Acta Sedimentologica Sinica 21, 96–105 (in Chinese with English abstract)

Fedonkin MA (1990) Systematic description of Vendian metazoa In The Vendian System: Vol. 1 Paleontology eds Sokolov BS and Iwanowski AB). pp. 71–120. Berlin, Germany: Springer-Verlag Berlin Heidelberg

Fedorov AB and Zhuravlev AY (1993) Oldest biomineralized animal Cloudina, in "Biomineralization 93". In 7th International Symposium on Biomineralization, Programs and Abstracts, November pp. 17–20.

Fike DA and Grotzinger JP (2008) A paired sulfate-pyrite $\delta^{34}S$ approach to understanding the evolution of the Ediacaran-Cambrian sulfur cycle. Geochimica et Cosmochimica Acta 72, 2636–2648. 10.1016/j.gca.2008.03.021

Gamper A, (2014) Global Trends in Nutrient Dynamics During the Ediacaran-Cambrian Period as Revealed by Nitrogen and Carbon Isotope Trends, Ph.D. Dissertation, Freie Universität Berlin, Berlin, Germany, 184 pp. https://d-nb.info/1064307035/34

Gamper A, Struck U, Ohnemueller F, Heubeck C and Hohl S (2015) Chemo- and biostratigraphy of the Gaojiashan section (northern Yangtze platform, South China): a new Pc-C boundary section. Fossil Record 18, 105–117. 10.5194/fr-18-105-2015

Ginsburg RN and James NP (1976) Submarine botryoidal aragonite in Holocene reef limestones, Belize. Geology 4, 431–436. 10.1130/0091-7613(1976)4<431:sbaihr>2.0.co;2

Gomez FJ, Kah LC, Bartley JK and Astini RA (2014) Microbialites in a high-altitude Andean lake: multiple controls in carbonate precipitation and lamina accretion. Palaios 29, 233–249. 10.2110/palo.2013.049

Gorin GE, Racz LG and Walter MR (1982) Late Precambrian-Cambrian sediments of Huqf Group, Sultanate of Oman. AAPG Bulletin 66, 2609–2627

Grant SWF (1990) Shell structure and distribution of *Cloudina*, a potential index fossil for the terminal Proterozoic. American Journal of Science 290-A, 261–294 [PubMed: 11538690]

Grant SWF, Knoll AH and Germs GJB (1991) Probable calcified metaphytes in the latest Proterozoic Nama Group, Namibia: origin, diagenesis, and implications. Journal of Paleontology 65, 1–18. 10.1017/s002233600002014x [PubMed: 11538648]

Grazhdankin DV, Balthasar U, Nagovitsin KE and Kochnev BB (2008) Carbonate-hosted Avalon-type fossils in arctic Siberia. Geology 36, 803–806. 10.1130/g24946a.1

Grotzinger J, Adams E and Schröder S (2005) Microbial-metazoan reefs of the terminal Proterozoic Nama Group (c. 550–543 Ma), Namibia. Geological Magazine 142, 499–517. 10.1017/s0016756805000907

Grotzinger J and Al-Rawahi Z (2014) Depositional facies and platform architecture of microbialite-dominated carbonate reservoirs, Ediacaran-Cambrian Ara Group, Sultanate of Oman. AAPG Bulletin 98, 1453–1494. 10.1306/02271412063

Grotzinger JP and James NP (2000) Precambrian carbonates: evolution of understanding In Carbonate Sedimentation and Diagenesis in the Evolving Precambrian World eds Grotzinger JP and James NP). pp. 3–20. Tulsa, Oklahoma, USA: Society for Sedimentary Geology (SEPM) Special Publication

Grotzinger JP, Watters WA and Knoll AH (2000) Calcified metazoans in thrombolite-stromatolite reefs of the terminal Proterozoic Nama Group, Namibia. Paleobiology 26, 334–359. 10.1666/0094-8373(2000)026<0334:cmitsr>2.0.co;2

Guo Q, Deng Y and Yang X (2012) Carbon isotopic evolution of the Late Ediacaran Gaojiashan biota on the northern Yangtze Platform, south China. Acta Geologica Sinica (English Edition) 86, 1447–1454. 10.1111/1755-6724.12013

Guo X and Chafetz HS (2014) Trends in $\delta^{18}O$ and $\delta^{13}C$ values in lacustrine tufa mounds: Palaeohydrology of Searles Lake, California. Sedimentology 61, 221–237. 10.1111/sed.12085

Habicht KS, Gade M, Thamdrup B, Berg P and Canfield DE (2002) Calibration of sulfate levels in the Archean ocean. Science 298, 2372–2374. 10.1126/science.1078265 [PubMed: 12493910]

Hall M, Kaufman AJ, Vickers-Rich P, Ivantsov A, Trusler P, Linnemann U, Hofmann M, Elliott D, Cui H, Fedonkin M, Hoffmann K-H, Wilson SA, Schneider G and Smith J (2013) Stratigraphy,

palaeontology and geochemistry of the late Neoproterozoic Aar Member, southwest Namibia: Reflecting environmental controls on Ediacara fossil preservation during the terminal Proterozoic in African Gondwana. Precambrian Research 238, 214–232. 10.1016/j.precamres.2013.09.009

Halverson GP, Dudás FÖ, Maloof AC and Bowring SA (2007) Evolution of the 87Sr/86Sr composition of Neoproterozoic seawater. Palaeogeography, Palaeoclimatology, Palaeoecology 256, 103–129. 10.1016/j.palaeo.2007.02.028

Halverson GP, Wade BP, Hurtgen MT and Barovich KM (2010) Neoproterozoic chemostratigraphy. Precambrian Research 182, 337–350. 10.1016/j.precamres.2010.04.007

Han J, Morris SC, Ou Q, Shu D and Huang H (2017) Meiofaunal deuterostomes from the basal Cambrian of Shaanxi (China). Nature 542, 228–231. 10.1038/nature21072 [PubMed: 28135722]

Hantsoo KG, Kaufman AJ, Cui H, Plummer RE and Narbonne GM (2018) Effects of bioturbation on carbon and sulfur cycling across the Ediacaran-Cambrian transition at the GSSP in Newfoundland, Canada. Canadian Journal of Earth Sciences 55, 1240–1252. 10.1139/cies-2017-0274

Hao Y, Zhou J, Chen X, Pan L, Hu Y and Hu A (2015) Genesis and geological significance of upper Sinian Dengying dolostone with grape-lace shaped cement, Sichuan Basin. Marine Origin Petroleum Geology 20, 57–64 (in Chinese with English abstract). 10.3969/j.issn. 1672-9854.2015.04.008

Hayes JM, Strauss H and Kaufman AJ (1999) The abundance of ^{13}C in marine organic matter and isotopic fractionation in the global biogeochemical cycle of carbon during the past 800 Ma. Chemical Geology 161, 103–125. 10.1016/s0009-2541(99)00083-2

Higgins J, Fischer W and Schrag D (2009) Oxygenation of the ocean and sediments: consequences for the seafloor carbonate factory. Earth and Planetary Science Letters 284, 25–33. 10.1016/j.epsl. 2009.03.039

Hofmann HJ and Mountjoy EW (2001) Namacalathus-Cloudina assemblage in Neoproterozoic Miette Group (Byng Formation), British Columbia: Canada's oldest shelly fossils. Geology 29, 1091–1094. 10.1130/0091-7613(2001)029<1091:ncainm>2.0.co;2

Horton TW, Defliese WF, Tripati AK and Oze C (2015) Evaporation induced 18O and 13C enrichment in lake systems: A global perspective on hydrologic balance effects. Quaternary Science Reviews 131, 365–379. 10.1016/j.quascirev.2015.06.030

Hua H, Chen Z and Yuan X (2007) The advent of mineralized skeletons in Neoproterozoic Metazoa—new fossil evidence from the Gaojiashan Fauna. Geological Journal 42, 263–279. 10.1002/gj.1077

Irwin H, Curtis C and Coleman M (1977) Isotopic evidence for source of diagenetic carbonates formed during burial of organic-rich sediments. Nature 269, 209–213. 10.1038/269209a0

Jacobsen SB and Kaufman AJ (1999) The Sr, C and O isotopic evolution of Neoproterozoic seawater. Chemical Geology 161, 37–57. 10.1016/s0009-2541(99)00080-7

Jiang G, Kennedy MJ and Christie-Blick N (2003) Stable isotopic evidence for methane seeps in Neoproterozoic postglacial cap carbonates. Nature 426, 822–826. 10.1038/nature02201 [PubMed: 14685234]

Jiang G, Kennedy MJ, Christie-Blick N, Wu H and Zhang S (2006a) Stratigraphy, sedimentary structures, and textures of the late Neoproterozoic Doushantuo cap carbonate in South China. Journal of Sedimentary Research 76, 978–995. 10.2110/jsr.2006.086

Jiang G, Shi X and Zhang S (2006b) Methane seeps, methane hydrate destabilization, and the late Neoproterozoic postglacial cap carbonates. Chinese Science Bulletin 51, 1152–1173. 10.1007/ s11434-006-1152-y

Jiang G, Kaufman AJ, Christie-Blick N, Zhang S and Wu H (2007) Carbon isotope variability across the Ediacaran Yangtze platform in South China: Implications for a large surface-to-deep ocean $\delta^{13}C$ gradient. Earth and Planetary Science Letters 261, 303–320. 10.1016/j.epsl.2007.07.009

Jiang G, Shi X, Zhang S, Wang Y and Xiao S (2011) Stratigraphy and paleogeography of the Ediacaran Doushantuo Formation (ca. 635–551Ma) in South China. Gondwana Research 19, 831–849. 10.1016/j.gr.2011.01.006

Jiang Y, Tao Y, Gu Y, Wang J, Qiang Z, Jiang N, Lin G and Jiang C (2016) Hydrothermal dolomitization in Dengying Formation, Gaoshiti-Moxi area, Sichuan Basin, SW China. Petroleum Exploration and Development 43, 54–64. 10.1016/S1876-3804(16)30006-4

Jørgensen BB and Kasten S (2006) Sulfur cycling and methane oxidation In Marine Geochemistry eds Schulz HD and Zabel M). pp. 271–309. Berlin: Springer-Verlag Berlin Heidelberg 10.1007/3-540-32144-6

Knauth LP and Kennedy MJ (2009) The late Precambrian greening of the Earth. Nature 460, 728–732. 10.1038/nature08213 [PubMed: 19587681]

Knoll AH, Grotzinger JP, Kaufman AJ and Kolosov P (1995) Integrated approaches to terminal Proterozoic stratigraphy: an example from the Olenek Uplift, northeastern Siberia. Precambrian Research 73, 251–270. 10.1016/0301-9268(94)00081-2 [PubMed: 11539551]

Lei H and Zhu L (1992) Study of origin of the Sinian algal and nonalgal dolomitites in Sichuan Basin. Acta Sedimentologica Sinica 10, 69–78 (in Chinese with English abstract)

Leleu T, Chavagnac V, Delacour A, Noiriel C, Ceuleneer G, Aretz M, Rommevaux C and Ventalon S (2016) Travertines associated with hyperalkaline springs: Evaluation as a proxy for paleoenvironmental conditions and sequestration of atmospheric CO_2. Journal of Sedimentary Research 86, 1328–1343. 10.2110/jsr.2016.79

Li D, Ling H-F, Shields-Zhou GA, Chen X, Cremonese L, Och L, Thirlwall M and Manning CJ (2013a) Carbon and strontium isotope evolution of seawater across the Ediacaran–Cambrian transition: Evidence from the Xiaotan section, NE Yunnan, South China. Precambrian Research 225, 128–147. 10.1016/j.precamres.2012.01.002

Li L, Tan X, Zeng W, Zhou T, Yang Y, Hong H, Luo B and Bian L (2013b) Development and reservoir significance of mud mounds in Sinian Dengying Formation, Sichuan Basin. Petroleum Exploration and Development 40, 714–721. 10.1016/s1876-3804(13)60096-8

Li W, Hu G and Zhou J (2015) Asphalt features and gas accumulation mechanism of Sinian reservoirs in the Tongwan Palaeo-uplift, Sichuan Basin. Natural Gas Industry B 2, 314–322. 10.1016/j.ngib.2015.09.004

Lian C, Qu F, Tan X, Li L, Jin M, Zeng W, Ren Q, Hu G and Liu H (2016) Occurrences and formation mechanisms of botryoidal structures from the Sinian Dengying Formation, Sichuan Basin, China. Acta Geologica Sinica (English Edition) 90, 384–385. 10.1111/1755-6724.12666

Lian C, Ren G, Qu F, Tan X, Li L, Zeng W, Hu G and Liu H (2017) Review and prospect on the botryoidal structures from the Sinian Dengying Formation, Sichuan Basin, China. Petroleum 3, 190–196. 10.1016/j.petlm.2016.12.001

Lin S, Zhang Y, Zhang L, Tao X and Wang M (1986) Body and trace fossils of metazoa and algal macrofossils from the upper Sinian Gaojiashan Formation in southern Shaanxi. Geology of Shaanxi 4, 9–17 (in Chinese with English abstract)

Lin X, Peng J, Yan J and Hou Z (2015) A discussion about origin of botryoidal dolostone of the Sinian Dengying Formation in Sichuan Basin. Journal of Palaeogeography 6, 755–770 (in Chinese with English abstract). 10.7605/gdlxb.2015.06.062

Lin Z, Wang Q, Feng D, Liu Q and Chen D (2011) Post-depositional origin of highly ^{13}C-depleted carbonate in the Doushantuo cap dolostone in South China: Insights from petrography and stable carbon isotopes. Sedimentary Geology 242, 71–79. 10.1016/j.sedgeo.2011.10.009

Linnemann U, Ovtcharova M, Schaltegger U, Gärtner A, Hautmann M, Geyer G, Vickers-Rich P, Rich T, Plessen B, Hofmann M, Zieger J, Krause R, Kriesfeld L and Smith J (2019) New high-resolution age data from the Ediacaran-Cambrian boundary indicate rapid, ecologically driven onset of the Cambrian explosion. Terra Nova, In press. 10.1111/ter.12368

Liu J, Yang P, Wang Z, Zhuo J and Du Q (2012) Paleo-weathering crust at the top of Sinian Dengying Formation in northern Guizhou and its petroleum exploration significance. Geology in China 4, 931–938 (in Chinese with English abstract)

Liu J, Li W, Zhang B, Zhou H, Yuan X, Shan X, Zhang J, Deng S, Gu Z, Fan R, Wang Y and Li X (2015) Sedimentary palaeogeography of the Sinian in Upper Yangtze Region. Journal of Palaeogeography 17, 735–753 (in Chinese with English abstract). 10.7605/gdlxb.2015.06.061

Liu S, Huang W, Jansa LF, Wang G, Song G, Zhang C, Sun W and Ma W (2014a) Hydrothermal dolomite in the Upper Sinian (Upper Proterozoic) Dengying Formation, east Sichuan Basin, China. Acta Geologica Sinica 88, 1466–1487. 10.1111/1755-6724.12312

Liu X, Fike D, Li A, Dong J, Xu F, Zhuang G, Rendle-Bühring R and Wan S (2019) Pyrite sulfur isotopes constrained by sedimentation rates: Evidence from sediments on the East China Sea

inner shelf since the late Pleistocene. Chemical Geology 505, 66–75. 10.1016/j.chemgeo.2018.12.014

Liu Y, Xiao S, Shao T, Broce J and Zhang H (2014b) The oldest known priapulid-like scalidophoran animal and its implications for the early evolution of cycloneuralians and ecdysozoans. Evolution & Development 16, 155–165. 10.1111/ede.12076 [PubMed: 24754444]

Lorens RB (1981) Sr, Cd, Mn and Co distribution coefficients in calcite as a function of calcite precipitation rate. Geochimica et Cosmochimica Acta 45, 553–561. 10.1016/0016-7037(81)90188-5

Loyd SJ, Marenco PJ, Hagadorn JW, Lyons TW, Kaufman AJ, Sour-Tovar F and Corsetti FA (2012) Sustained low marine sulfate concentrations from the Neoproterozoic to the Cambrian: Insights from carbonates of northwestern Mexico and eastern California. Earth and Planetary Science Letters 339–340, 79–94. 10.1016/j.epsl.2012.05.032

Loyd SJ, Marenco PJ, Hagadorn JW, Lyons TW, Kaufman AJ, Sour-Tovar F and Corsetti FA (2013) Local δ34S variability in ~580Ma carbonates of northwestern Mexico and the Neoproterozoic marine sulfate reservoir. Precambrian Research 224, 551–569. 10.1016/j.precamres.2012.10.007

Lu M, Zhu M, Zhang J, Shields-Zhou G, Li G, Zhao F, Zhao X and Zhao M (2013) The DOUNCE event at the top of the Ediacaran Doushantuo Formation, South China: Broad stratigraphic occurrence and non-diagenetic origin. Precambrian Research 225, 86–109. 10.1016/j.precamres.2011.10.018

Luo C, Pan B and Reitner J (2017) Chambered structures from the Ediacaran Dengying Formation, Yunnan, China: comparison with the Cryogenian analogues and their microbial interpretation. Geological Magazine 154, 1269–1284. 10.1017/s001675681700053x

Macdonald FA, McClelland WC, Schrag DP and Macdonald WP (2009) Neoproterozoic glaciation on a carbonate platform margin in Arctic Alaska and the origin of the North Slope subterrane. Geological Society of America Bulletin 121, 448–473. 10.1130/b26401.1

Mason R, Li Y, Cao K, Long Y and She Z-B (2017) Ediacaran macrofossils in Shunyang Valley, Sixi, Three Gorges District, Hubei Province, China. Journal of Earth Science 28, 614–621. 10.1007/s12583-017-0773-1

Mazzullo SJ and Cys JM (1979) Marine aragonite sea-floor growths and cements in Permian phylloid algal mounds, Sacramento Mountains, New Mexico. Journal of Sedimentary Research 49, 917–936. 10.1306/212f7879-2b24-11d7-8648000102c1865d

Mazzullo SJ (1980) Calcite pseudospar replacive of marine acicular aragonite, and implications for aragonite cement diagenesis. Journal of Sedimentary Research 50, 409–422. 10.1306/212f7a18-2b24-11d7-8648000102c1865d

Mcfadden KA, Huang J, Chu X, Jiang G, Kaufman AJ, Zhou C, Yuan X and Xiao S (2008) Pulsed oxidation and biological evolution in the Ediacaran Doushantuo Formation. Proceedings of the National Academy of Sciences 105, 3197–3202. 10.1073/pnas.0708336105

Meister P, Mckenzie JA, Vasconcelos C, Bernasconi S, Frank M, Gutjahr M and Schrag DP (2007) Dolomite formation in the dynamic deep biosphere: results from the Peru Margin. Sedimentology 54, 1007–1032. 10.1111/j.1365-3091.2007.00870.x

Meng F, Ni P, Schiffbauer JD, Yuan X, Zhou C, Wang Y and Xia M (2011) Ediacaran seawater temperature: Evidence from inclusions of Sinian halite. Precambrian Research 184, 63–69. 10.1016/j.precamres.2010.10.004

Meyer M, Schiffbauer JD, Xiao S, Cai Y and Hua H (2012) Taphonomy of the upper Ediacaran enigmatic ribbonlike fossil Shaanxilithes. Palaios 27, 354–372. 10.2110/palo.2011.p11-098r

Mo J, Wang X, Leng S, Lin G, Xiong J, Xie L and Zhou Z (2013) Reservoir characteristics and control Factors of Sinian Denying Formation in central Sichuan. Geology in China 40, 1505–1513 (in Chinese with English abstract)

Mou C, Wang X, Liang W, Wang Y and Men X (2015) Characteristics and genesis of grape-like stone of dolomite in Sinian Dengying Formation in Yangtze region:A case from the first section of Dengying Formation in Yangba, Nanjiang, Sichuan Province. Acta Sedimentologica Sinica 33, 1097–1110 (in Chinese with English abstract). 10.14027/j.cnki.cixb.2015.06.004

Nagovitsin KE, Rogov VI, Marusin VV, Karlova GA, Kolesnikov AV, Bykova NV and Grazhdankin DV (2015) Revised Neoproterozoic and Terreneuvian stratigraphy of the Lena-Anabar Basin and

north-western slope of the Olenek Uplift, Siberian Platform. Precambrian Research 270, 226–245. 10.1016/j.precamres.2015.09.012

Narbonne G (2018) Terminal Ediacaran Stage Working Group Results of the First Ballot – July 2018. 6 pp.

Narbonne GM (2005) The Ediacara Biota: Neoproterozoic origin of animals and their ecosystems. Annual Review of Earth and Planetary Sciences 33, 421–442. 10.1146/annurev.earth.33.092203.122519

Narbonne GM, Xiao S, Shields GA and Gehling JG (2012) The Ediacaran Period. In The Geologic Time Scale eds Gradstein FM, Ogg JG, Schmitz MD and Ogg GM). pp. 413–435. Boston, USA: Elsevier 10.1016/b978-0-444-59425-9.00018-4

Oehlert AM and Swart PK (2014) Interpreting carbonate and organic carbon isotope covariance in the sedimentary record. Nature Communications 5, 4672 10.1038/ncomms5672

Pasquier V, Sansjofre P, Rabineau M, Revillon S, Houghton J and Fike DA (2017) Pyrite sulfur isotopes reveal glacial-interglacial environmental changes. Proceedings of the National Academy of Sciences 114, 5941–5945. 10.1073/pnas.1618245114

Pelechaty SM, Grotzinger JP, Kashirtsev VA and Zhernovsky VP (1996a) Chemostratigraphic and sequence stratigraphic constraints on Vendian-Cambrian basin dynamics, northeast Siberian craton. The Journal of Geology 104, 543–563. 10.1086/629851

Pelechaty SM, Kaufman AJ and Grotzinger JP (1996b) Evaluation of δ13C chemostratigraphy for intrabasinal correlation: Vendian strata of northeast Siberia. Geological Society of America Bulletin 108, 992–1003. 10.1130/0016-7606(1996)108<0992:eoccfi>2.3.co;2

Peng J, Zhang H and Lin X (2017) Study on characteristics and genesis of botryoidal dolostone of the Upper Sinian Dengying Formation: a case study from Hanyuan region, Sichuan, China. Carbonates and Evaporites 33, 285–299. 10.1007/s13146-017-0343-8

Penny A, Wood R, Curtis A, Bowyer F, Tostevin R and Hoffman K-H (2014) Ediacaran metazoan reefs from the Nama Group, Namibia. Science 344, 1504–1506. 10.1126/science.1253393 [PubMed: 24970084]

Peters SE and Gaines RR (2012) Formation of the 'Great Unconformity' as a trigger for the Cambrian explosion. Nature 484, 363–366. 10.1038/nature10969 [PubMed: 22517163]

Pierre C, Blanc-Valleron MM, Caquineau S, März C, Ravelo AC, Takahashi K and Alvarez Zarikian C (2016) Mineralogical, geochemical and isotopic characterization of authigenic carbonates from the methane-bearing sediments of the Bering Sea continental margin (IODP Expedition 323, Sites U1343-U1345). Deep Sea Research Part II: Topical Studies in Oceanography 125–126, 133–144. 10.1016/j.dsr2.2014.03.011

Pruss SB, Corsetti FA and Fischer WW (2008) Seafloor-precipitated carbonate fans in the Neoproterozoic Rainstorm Member, Johnnie Formation, Death Valley Region, USA. Sedimentary Geology 207, 34–40. 10.1016/j.sedgeo.2008.03.005

Purser BH, Tucker ME and Zenger DH (2009) Dolomites: A Volume in Honor of Dolomieu. John Wiley & Sons.

Qian Y, He Z, Li H, Chen Y, Jin T, Sha X and Li H (2017) Discovery and discussion on origin of botryoidal dolostone in the Upper Sinian in North Tarim Basin. Journal of Palaeogeography 19, 197–210 (in Chinese with English abstract). 10.7605/gdlxb.2017.02.016

Ries JB, Fike DA, Pratt LM, Lyons TW and Grotzinger JP (2009) Superheavy pyrite (δ34Spyr > δ34Scas) in the terminal Proterozoic Nama Group, southern Namibia: A consequence of low seawater sulfate at the dawn of animal life. Geology 37, 743–746. 10.1130/q25775a.1

Rogov VI, Marusin V, Bykova NV, Goy Y, Nagovitsin KE, Kochnev BB, Karlova G and Grazhdankin DV (2012) The oldest evidence of bioturbation on Earth. Geology 40, 395–398. https://doi.Org/10.1130/g32807.1

Rogov VI, Marusin V, Bykova N, Goy Y, Nagovitsin K, Kochnev B, Karlova G and Grazhdankin DV (2013a) The oldest evidence of bioturbation on Earth: Reply. Geology 41, e290 10.1130/g34237y.1

Rogov VI, Marusin V, Bykova NV, Goy Y, Nagovitsin KE, Kochnev BB, Karlova G and Grazhdankin DV (2013b) The oldest evidence of bioturbation on Earth: Reply. Geology 41, e300 https://doi.orq/10.1130/q34594v.1

Rogov VI, Karlova GA, Marusin VV, Kochnev BB, Nagovitsin KE and Grazhdankin DV (2015) Duration of the first biozone in the Siberian hypostratotype of the Vendian. Russian Geology and Geophysics 56, 573–583. 10.1016/j.rgg.2015.03.016

Sandberg P (1985) Aragonite cements and their occurrence in ancient limestones In Carbonate Cements eds Schneidermann N and Harris PM). pp. 33–57. Tulsa, Oklahoma, USA: The Society of Economic Paleontologists and Mineralogists (SEPM) Special Publication 10.2110/pec.85.36.0033

Sawaki Y, Ohno T, Tahata M, Komiya T, Hirata T, Maruyama S, Windley BF, Han J, Shu D and Li Y (2010) The Ediacaran radiogenic Sr isotope excursion in the Doushantuo Formation in the Three Gorges area, South China. Precambrian Research 176, 46–64. 10.1016/j.precamres.2009.10.006

Saylor BZ, Kaufman AJ, Grotzinger JP and Urban F (1998) A composite reference section for terminal Proterozoic strata of southern Namibia. Journal of Sedimentary Research 68, 1223–1235. 10.2110/jsr.68.1223 [PubMed: 11758565]

Schrag DP, Higgins JA, Macdonald FA and Johnston DT (2013) Authigenic carbonate and the history of the global carbon cycle. Science 339, 540–543. 10.1126/science.1229578 [PubMed: 23372007]

Shen B, Xiao S, Zhou C and Yuan X (2009) Yangtziramulus zhangi new genus and species, a carbonate-hosted macrofossil from the Ediacaran Dengying Formation in the Yangtze Gorges area, South China. Journal of Paleontology 83, 575–587. 10.1666/08-042r1.1

Shen B, Xiao S, Zhou C, Dong L, Chang J and Chen Z (2017) A new modular palaeopascichnid fossil *Curviacus ediacaranus* new genus and species from the Ediacaran Dengying Formation in the Yangtze Gorges area of South China. Geological Magazine 154, 1257–1268. 10.1017/s001675681700036X

Shi Z, Liang P, Wang Y, Hu X, Tian Y and Wang C (2011) Geochemical characterishcs and genesis of grapestone in Sinian Dengying Formation in southeastern Sichuan basin. Acta Petmlogica Sinica 27, 2263–2271 (in Chinese with English abstract)

Shi Z, Wang Y, Tian Y and Wang C (2013) Cementation and diagenetic fluid of algal dolomites in the Sinian Dengying Formation in southeastern Sichuan Basin. Science China: Earth Sciences 56, 192–202. 10.1007/s11430-012-4541-x

Si C, Hao Y, Zhou J, Ni C and Pan L (2014) Characteristics and controlling factors of reservoir in Sinian Dengying Formation, Sichuan Basin. Journal of Chengdu University of Technology(Science & Technology Edition) 41, 266–273 (in Chinese with English abstract). 10.3969/j.issn.1671-9727.2014.03.02

Siegmund H and Erdtmann B-D (1994) Facies and diagenesis of some Upper Proterozoic dolomites of South China. Facies 31, 255–263. 10.1007/bf02536942

Spötl C (2011) Long-term performance of the Gasbench isotope ratio mass spectrometry system for the stable isotope analysis of carbonate microsamples. Rapid Communications in Mass Spectrometry 25, 1683–1685. 10.1002/rcm.5037 [PubMed: 21594944]

Steiner M, Li G, Qian Y and Zhu M (2004) Lower Cambrian small shelly fossils of northern Sichuan and southern Shaanxi (China), and their biostratigraphic importance. Geobios 37, 259–275. 10.1016/j.geobios.2003.08.001

Sun W (1986) Late Precambrian pennatulids (sea pens) from the eastern Yangtze Gorge, China: Paracharnia gen. nov. Precambrian Research 31, 361–375. 10.1016/0301-9268(86)90040-9

Talbot M and Kelts K (1986) Primary and diagenetic carbonates in the anoxic sediments of Lake Bosumtwi, Ghana. Geology 14, 912–916. 10.1130/0091-7613(1986)14<912:padcit>2.0.co;2

Tan X, Xiao D, Chen J, Li L and Liu H (2015) New advance and enlightenment of eogenetic karstification. Journal of Palaeogeography 17, 441–456 (in Chinese with English abstract). 10.7605/gdlxb.2015.04.037

Tostevin R, He T, Turchyn AV, Wood RA, Penny AM, Bowyer F, Antler G and Shields GA (2017) Constraints on the late Ediacaran sulfur cycle from carbonate associated sulfate. Precambrian Research 290, 113–125. 10.1016/j.precamres.2017.01.004

Tucker ME (1982) Precambrian dolomites: petrographic and isotopic evidence that they differ from Phanerozoic dolomites. Geology 10, 7–12. 10.1130/0091-7613(1982)10<7:PDPAIE>2.0.CO;2

Tucker ME (1983) Diagenesis, geochemistry, and origin of a Precambrian dolomite: the Beck Spring Dolomite of eastern California. Journal of Sedimentary Research 53, 1097–1119. 10.1306/212f8323-2b24-11d7-8648000102c1865d

Tucker ME (2009) Sedimentary Petrology: An Introduction to the Origin of Sedimentary Rocks. Blackwell Science Ltd, 262 pp.

Ufnar DF, Gröcke DR and Beddows PA (2008) Assessing pedogenic calcite stable-isotope values: Can positive linear covariant trends be used to quantify palaeo-evaporation rates? Chemical Geology 256, 46–51. 10.1016/j.chemgeo.2008.07.022

Vishnevskaya IA, Letnikova EF, Vetrova NI, Kochnev BB and Dril SI (2017) Neoproterozoic sedimentary rocks of Khorbusuonka Group (Olenek Uplift, Russia): Chemostratigraphy and U-Pb dating of detrital zircons by LA ICP-MS method. Gondwana Research 51, 255–271. 10.1016/j.gr.2017.07.010

Wang G, Liu S, Ma Y, Xu G and Cai X (2010) Characteristics of subaerial karstification and late reconstruction in the Dengying Formation, Sichuan basin, southwestern China. Journal of Earth Science 21, 290–302. 10.1007/s12583-010-0093-1

Wang S and Xiang F (1999) The origin of the dolostones from the Sinian Dengying Formation in the Ziyang district, Sichuan. Sedimentary Facies and Palaeogeography 19, 21–29 (in Chinese with English abstract)

Wang W, Zhou C, Yuan X, Chen Z and Xiao S (2012) A pronounced negative δ13C excursion in an Ediacaran succession of western Yangtze Platform: A possible equivalent to the Shuram event and its implication for chemostratigraphic correlation in South China. Gondwana Research 22, 1091–1101. 10.1016/j.gr.2012.02.017

Wang W, Yang Y, Wen L, Luo B, Luo W, Xia M and Sun S (2016) A study of sedimentary characteristics of microbial carbonate: A case study of the Sinian Dengying Formation in Gaomo area, Sichuan Basin. Geology in China 43, 306–318 (in Chinese with English abstract). 10.12029/gc20160123

Wang X, Mu S, Fang S, Huang J and Hou F (2000) Evolution of porosity in the process of Sinian dolostone diagenesis in Southwest Sichuan. Acta Sedimentologica Sinica 18, 549–554 (in Chinese with English abstract)

Wang X, Shi X, Jiang G and Tang D (2014a) Organic carbon isotope gradient and ocean stratification across the late Ediacaran-Early Cambrian Yangtze Platform. Science China: Earth Sciences 57, 919–929. 10.1007/s11430-013-4732-0

Wang Z, Jiang H, Wang T, Lu W, Gu Z, Xu A, Yang Y and Xu Z (2014b) Paleo-geomorphology formed during Tongwan tectonization in Sichuan Basin and its significance for hydrocarbon accumulation. Petroleum Exploration and Development 41, 338–345. 10.1016/S1876-3804(14)60038-0

Warren LV, Fairchild TR, Gaucher C, Boggiani PC, Poire DG, Anelli LE and Inchausti JC (2011) Corumbella and in situ Cloudina in association with thrombolites in the Ediacaran Itapucumi Group, Paraguay. Terra Nova 23, 382–389. 10.1111/M365-3121.2011.01023.x

Wehrmann LM, Risgaard-Petersen N, Schrum HN, Walsh EA, Huh Y, Ikehara M, Pierre C, D'hondt S, Ferdelman TG, Ravelo AC, Takahashi K and Zarikian CA (2011) Coupled organic and inorganic carbon cycling in the deep subseafloor sediment of the northeastern Bering Sea Slope (IODP Exp. 323). Chemical Geology 284, 251–261. 10.1016/j.chemgeo.2011.03.002

Wei G-Y, Planavsky NJ, Tarhan LG, Chen X, Wei W, Li D and Ling H-F (2018) Marine redox fluctuation as a potential trigger for the Cambrian explosion. Geology 46, 587–590. 10.1130/G40150.1

Wen L, Wang W, Zhang J and Luo B (2017) Classification of Sinian Dengying Formation and sedimentary evolution mechanism of Gaoshiti-Moxi area in central Sichuan Basin. Acta Petrologica Sinica 33, 1285–1294 (in Chinese with English abstract)

Wood R (2016) Palaeoecology of Ediacaran Metazoan Reefs In Geological Society, London, Special Publications eds Brasier AT, Mcllroy D and McLoughlin N). pp. 195–210. Earth System

Evolution and Early Life: a Celebration of the Work of Martin Brasier.: Geological Society, London, Special Publications. 10.1144/sp448.1

Wood R, Ivantsov AY and Zhuravlev AY (2017a) First macrobiota biomineralization was environmentally triggered. Proceedings of the Royal Society B: Biological Sciences 284, 20170059 10.1098/rspb.2017.0059

Wood RA, Grotzinger JP and Dickson J (2002) Proterozoic modular biomineralized metazoan from the Nama Group, Namibia. Science 296, 2383–2386. 10.1126/science.1071599 [PubMed: 12089440]

Wood RA, Poulton SW, Prave AR, Hoffmann KH, Clarkson MO, Guilbaud R, Lyne JW, Tostevin R, Bowyer F, Penny AM, Curtis A and Kasemann SA (2015) Dynamic redox conditions control late Ediacaran metazoan ecosystems in the Nama Group, Namibia. Precambrian Research 261, 252–271. 10.1016/j.precamres.2015.02.004

Wood RA, Zhuravlev AY, Sukhov SS, Zhu M and Zhao F (2017b) Demise of Ediacaran dolomitic seas marks widespread biomineralization on the Siberian Platform. Geology 45, 27–30. 10.1130/g38367.1

Wray JL and Daniels F (1957) Precipitation of calcite and aragonite. Journal of the American Chemical Society 79, 2031–2034. 10.1021/ja01566a001

Xi X (1987) Characteristic and Environments of Sinian Evaporite in Southern Sichuan, China In Lecture Notes in Earth Sciences: Evaporite Basins (ed Peryt TM). pp. 23–29. Berlin: SpringerVerlag Berlin Heidelberg 10.1007/bfb0010098

Xiang F, Cheng H and Zhang J (2001) Paleokarst and its characteristics of Dengying Formation in Ziyang area. Acta Sedimentologica Sinica 19, 421–424 (in Chinese with English abstract)

Xiao S, Shen B, Zhou C, Xie G and Yuan X (2005) A uniquely preserved Ediacaran fossil with direct evidence for a quilted bodyplan. Proceedings of the National Academy of Sciences of the United States of America 102, 10227–10232. 10.1073/pnas.0502176102 [PubMed: 16014417]

Xiao S, Narbonne GM, Zhou C, Laflamme M, Grazhdankin DV, Moczydtowska-Vidal M and Cui H (2016) Toward an Ediacaran time scale: Problems, protocols, and prospects. Episodes 39, 540–555. 10.18814/epiiugs/2016/v39i4/103886

Xue Y, Cao R, Tang T, Yin L, Yu C and Yang J (2001) The Sinian stratigraphic sequence of the Yangtze region and correlation to the late Precambrian strata of North China. Journal of Stratigraphy 25, 207–234 (in Chinese with English abstract)

Yang S, Chen H, Zhong Y, Zhu X, Chen A, Wen H, Xu S and Wu C (2017) Microbolite of Late Sinian and its response for Tongwan Movement episode I in Southwest Sichuan, China. Acta Petrologica Sinica 33, 1148–1158 (in Chinese with English abstract)

Zhang F, Xiao S, Kendall B, Romaniello SJ, Cui H, Meyer M, Gilleaudeau GJ, Kaufman AJ and Anbar AD (2018) Extensive marine anoxia during the terminal Ediacaran Period. Science Advances 4, eaan8983 10.1126/sciadv.aan8983 [PubMed: 29938217]

Zhang H, Xiao S, Liu Y, Yuan X, Wan B, Muscente AD, Shao T, Gong H and Cao G (2015) Armored kinorhynch-like scalidophoran animals from the early Cambrian. Scientific reports 5, 16521 10.1038/srep16521 [PubMed: 26610151]

Zhang J, Jones B, Pan L, Zhou J, Qin Y, Hao Y and Wu M (2014a) Origin of botryoidal dolostone of the Sinian Dengying Formation in Sichuan Basin. Journal of Palaeogeography 16, 715–725 (in Chinese with English abstract). 10.7605/gdlxb.2014.05.057

Zhang L (1986) A discovery and preliminary study of the late stage of late Gaojiashan biota from Sinian in Ningqiang County, Shaanxi. Bulletin of the Xi'an Institute of Geology and Mineral Resources, Chinese Academy of Geological Sciences 13, 67–88 (in Chinese with English abstract)

Zhang P, Hua H and Liu W (2014b) Isotopic and REE evidence for the paleoenvironmental evolution of the late Ediacaran Dengying Section, Ningqiang of Shaanxi Province, China. Precambrian Research 242, 96–111. 10.1016/j.precamres.2013.12.011

Zhang T, Chu X, Zhang Q, Feng L and Huo W (2004) The sulfur and carbon isotopic records in carbonates of the Dengying Formation in the Yangtze Platform, China. Acta Petrologica Sinica 20, 717–724 (in Chinese with English abstract)

Zhang Y (1980) Origin of the botroydal textures in the Sinian dolostones. Petroleum Geology & Experiment 4, 40–43 (in Chinese)

Zhou C and Xiao S (2007) Ediacaran $\delta^{13}C$ chemostratigraphy of South China. Chemical Geology 237, 89–108. 10.1016/j.chemgeo.2006.06.021

Zhou C, Guan C, Cui H, Ouyang Q and Wang W (2016) Methane-derived authigenic carbonate from the lower Doushantuo Formation of South China: Implications for seawater sulfate concentration and global carbon cycle in the early Ediacaran ocean. Palaeogeography, Palaeoclimatology, Palaeoecology 461, 145–155. 10.1016/j.palaeo.2016.08.017

Zhou C, Yuan X, Xiao S, Chen Z and Hua H (2018) Ediacaran integrative stratigraphy and timescale of China. Science China Earth Sciences 62, 7–24. 10.1007/s11430-017-9216-2

Zhu D, Jin Z, Sun D, Peng Y, Zhang R and Yuan Y (2014a) Hydrothermally dolomitized reservoir bed in Sinian Dengying Formation, northern China: An example from Central Guizhou Uplift. Chinese Journal of Geology 49, 161–175 (in Chinese with English abstract). 10.3969/j.issn. 0563-5020.2014.01.012

Zhu D, Jin Z, Zhang R, Zhang D, He Z and Li S (2014b) Characteristics and developing mechanism of Sinian Dengying Formation dolomite reservoir with multi-stage karst. Earth Science Frontiers 21, 335–345 (in Chinese with English abstract). 10.13745/j.esf.2014.06.032

Zhu D, Zhang D, Li S, Feng J, Sun D, Lin J and Zhang R (2015) Development genesis and characteristics of karst reservoirs in lower assemblage in Sichuan Basin. Marine Origin Petroleum Geology 1, 33–44 (in Chinese with English abstract). 10.3969/j.issn. 1672-9854.2015.01.005

Zhu M, Zhang J and Yang A (2007) Integrated Ediacaran (Sinian) chronostratigraphy of South China. Palaeogeography, Palaeoclimatology, Palaeoecology 254, 7–61. 10.1016/j.palaeo.2007.03.025

Zhu M, Lu M, Zhang J, Zhao F, Li G, Yang A, Zhao X and Zhao M (2013) Carbon isotope chemostratigraphy and sedimentary facies evolution of the Ediacaran Doushantuo Formation in western Hubei, South China. Precambrian Research 225, 7–28. 10.1016/j.precamres.2011.07.019

Zhuravlev AY and Wood RA (2008) Eve of biomineralization: Controls on skeletal mineralogy. Geology 36, 923–926. 10.1130/g25094a.1

Zhuravlev AY, Liñán E, Vintaned JaG, Debrenne F and Fedorov AB (2012) New finds of skeletal fossils in the terminal Neoproterozoic of the Siberian Platform and Spain. Acta Palaeontologica Polonica 57, 205–224. 10.4202/app.2010.0074

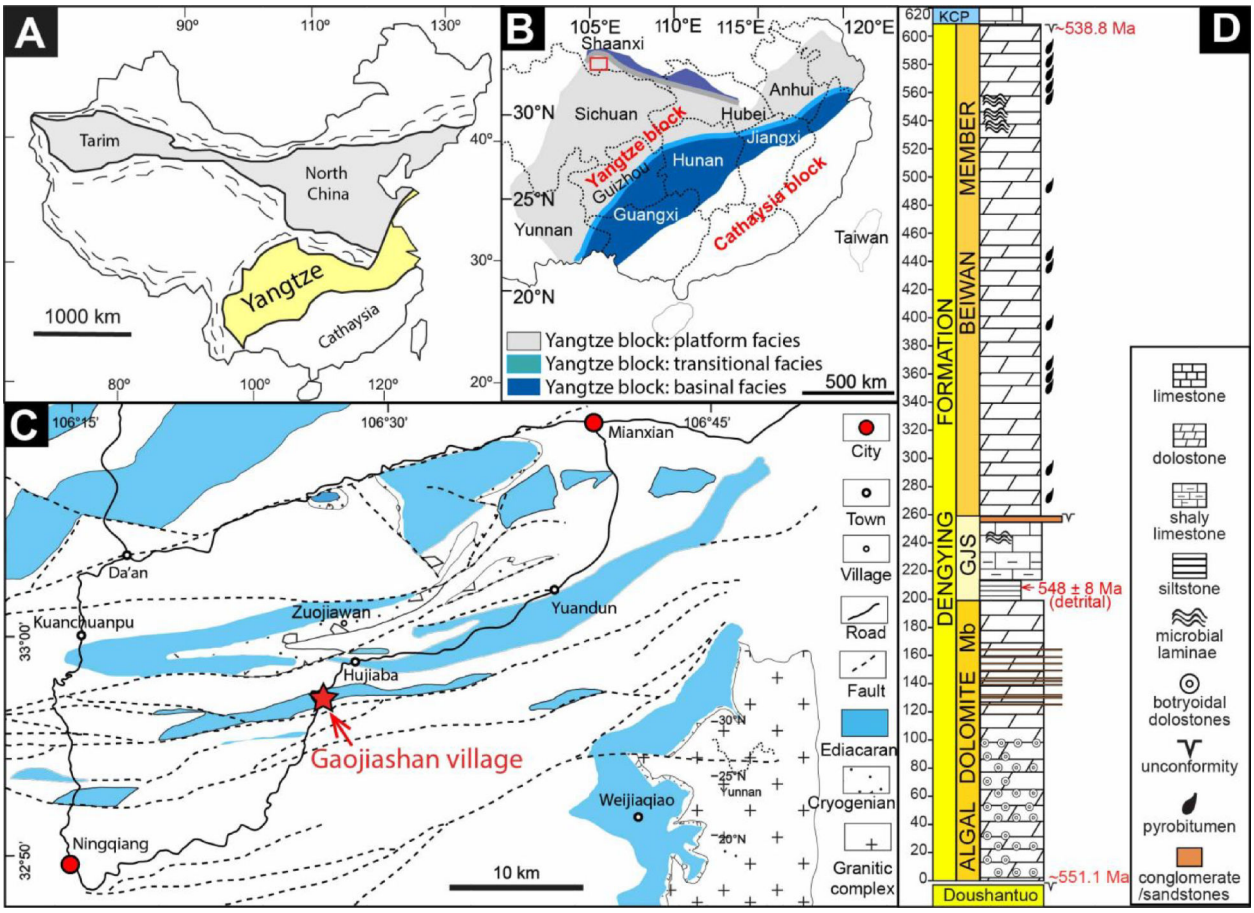

Figure 1.

Simplified tectonic map, geological map, litho- and chemo-stratigraphy of the terminal Ediacaran Dengying Formation at the Gaojiashan section, South China. (**A**) Tectonic framework of China, with the Yangtze Craton highlighted in yellow. (**B**) Ediacaran depositional environments on the Yangtze Craton (Jiang et al., 2007). Rectangle showing the location of the Ningqiang area in the northwestern margin of the Yangtze Platform. (**C**) Geological map of the Gaojiashan area in southern Shaanxi Province, modified after Cai et al. (2014). Red star indicates the studied section at the Gaojiashan village, Niqiang county, Hanzhong city, southern Shaanxi Province. (**D**) Simplified stratigraphy of the Dengying Formation at Gaojiashan (Cui et al., 2016b). Source of age data: (Condon et al., 2005; Cui et al., 2016b; Linnemann et al., 2019). Abbreviations: Cam = Cambrian Period, GJS = Gaojiashan Member, KCP = Kuanchuanpu Formation, GJB = Guojiaba Formation.

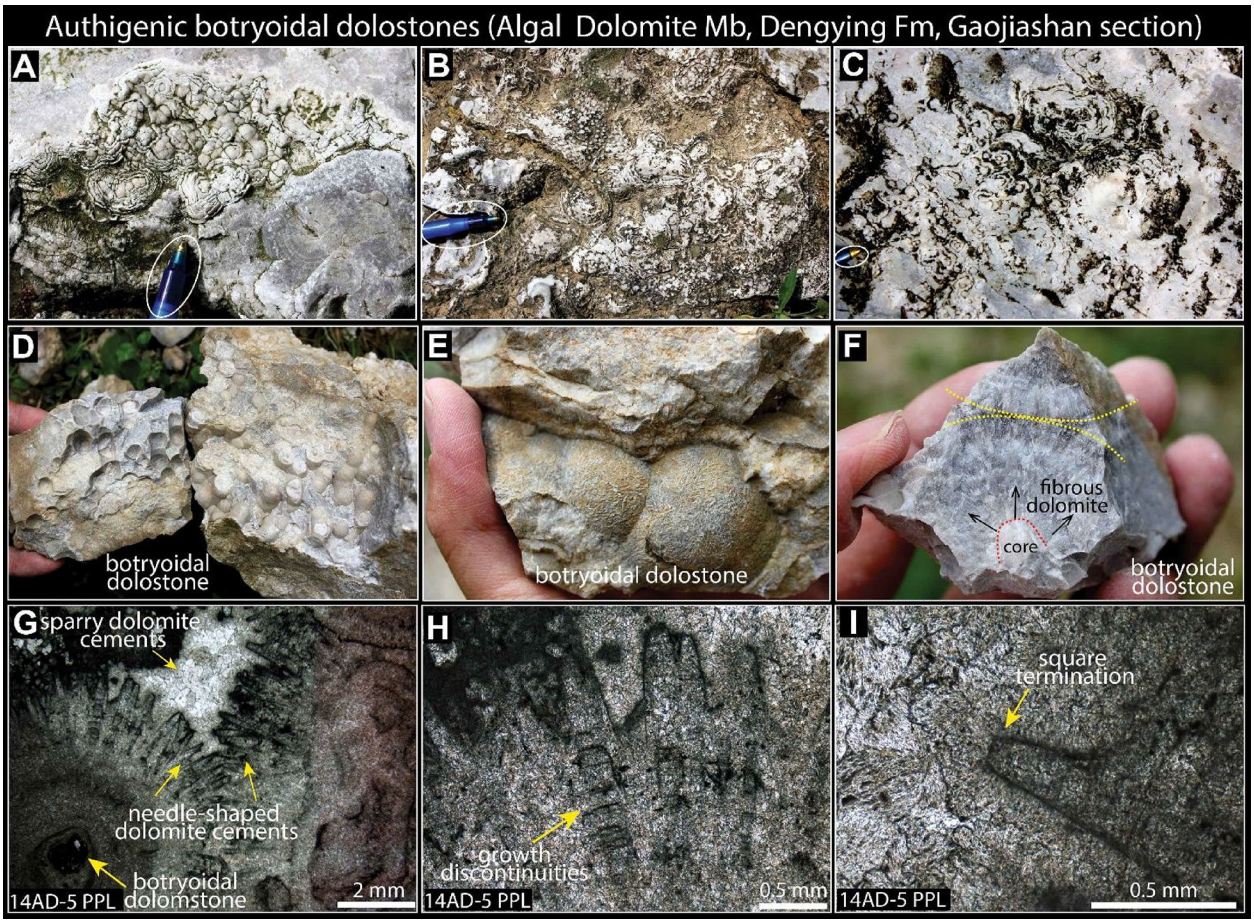

Figure 2.

Field and microscopic views of the authigenic botryoidal dolostones that are typical in the lower half of the Algal Dolomite Member of the Dengying Formation at the Gaojiashan section. (**A-C**) Outcrops showing distinct botryoidal textures with concentric lamina. Pen for scale. (**D-E**) Hand samples showing the distinct botryoidal texture. Note the part and counterpart in **D**. (**F**) Fresh fracture surface showing radial fabrics diverging from the core. (**G**) Microscopic images of the authigenic botryoidal dolostone showing needle-shaped crystals with growth discontinuities and square terminations. Note the needle-shaped crystals as the first-stage cements and the sparry dolomite as the second-stage cements. (**H-I**) Closer views of the needle-shaped crystals with discontinuities and square terminations, indicating originally aragonite in mineralogy. PPL = plane polarized light.

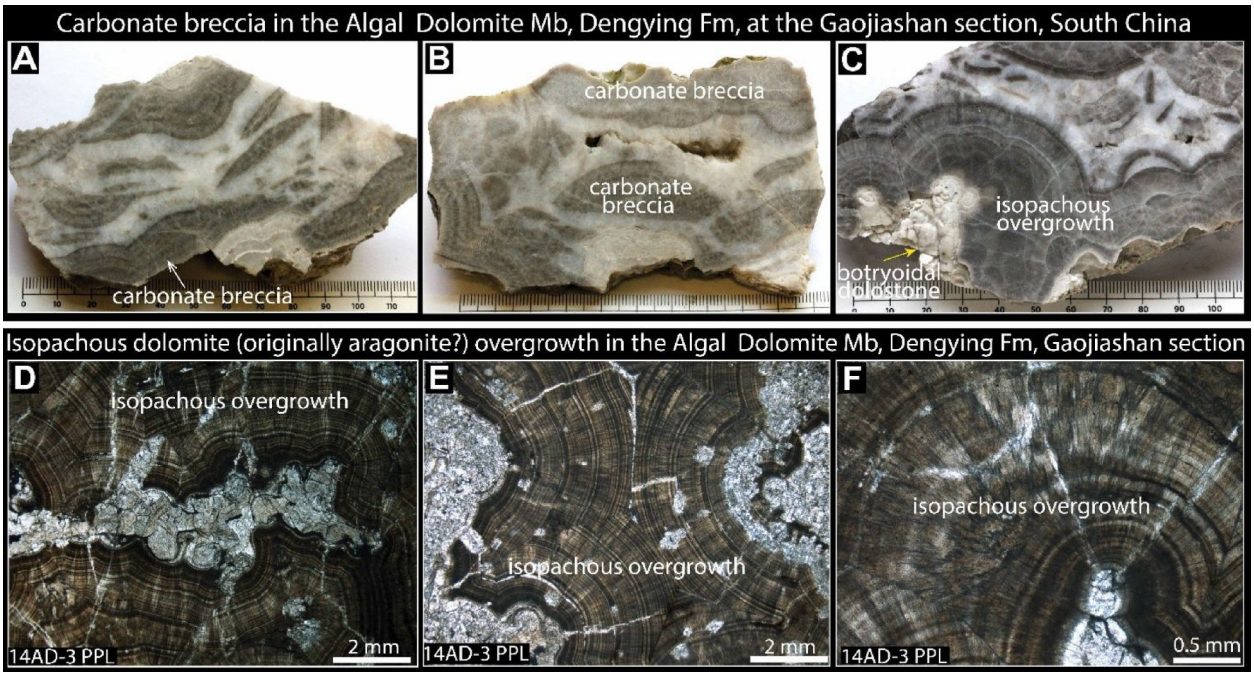

Figure 3.

Field samples and microscopic views of the carbonate breccia and isopachous overgrowth that are typical in the lower half of the Algal Dolomite Member of the Dengying Formation at the Gaojiashan section. (**A-C**) Karst breccia cemented by carbonates in the vugs between breccias. Scale in millimeters. (**D-F**) Petrographic images of sample 14AD-3, showing isopachous void-filling carbonate cements with concentric textures (brown color) surrounding coarse dolomite sediments (white color). PPL: plane polarized light.

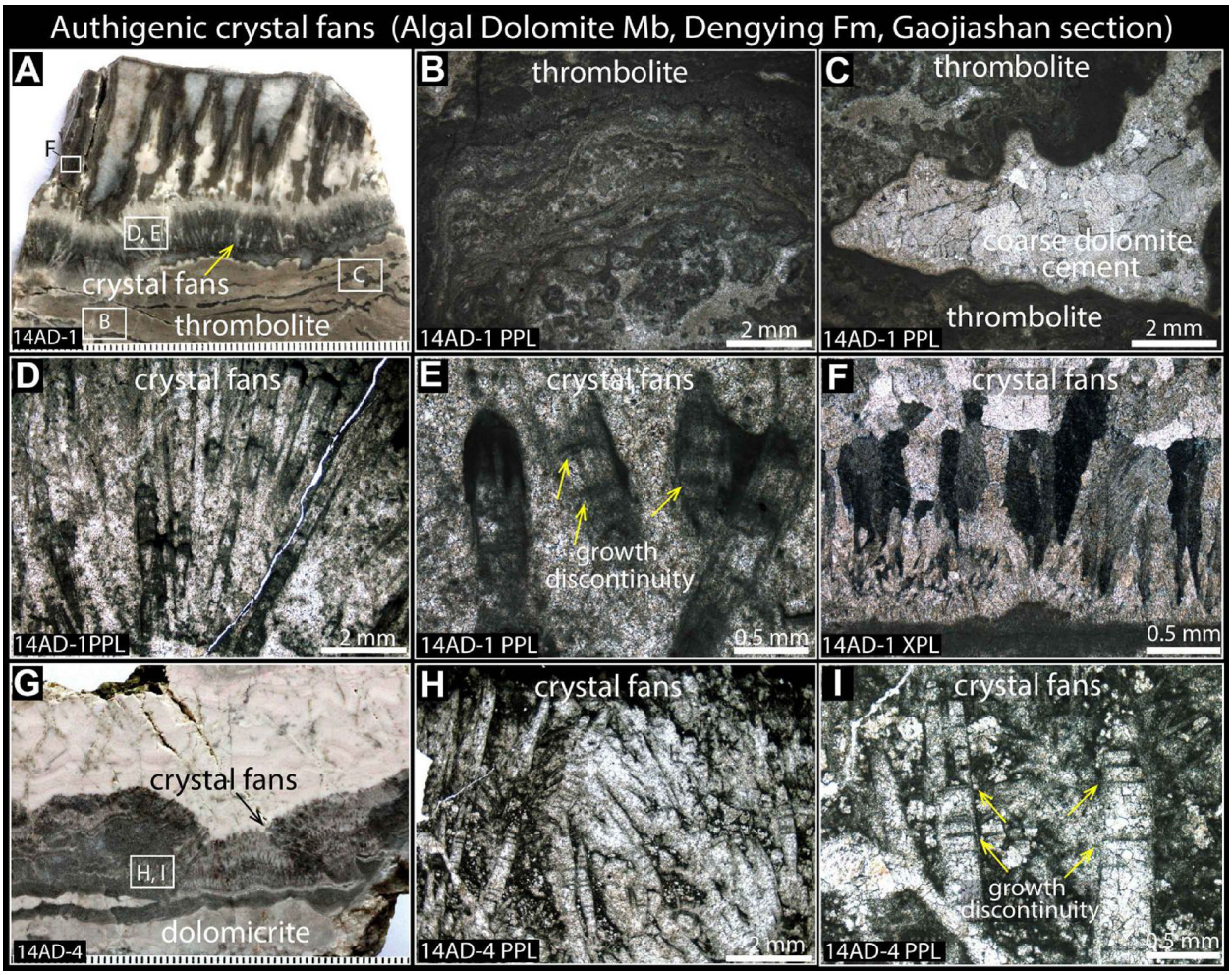

Figure 4.

Hand samples and microscopic views of the thrombolite and authigenic aragonite (now dolomite) crystal fans that are typical in the lower half of the Algal Dolomite Member of the Dengying Formation at the Gaojiashan section. (**A**) Sample slab 14AD-1, showing thrombolite sediments in the lower part and two generations of crystal fans in the middle and upper parts, respectively. Scale in millimeters. (**B-C**) Closer views of thrombolitic texture in labelled rectangles in **A**. Note the coarse dolomite cements within a large void of the thrombolitic dolomite matrix. (**D-E**) Authigenic crystal fans in labelled rectangles in **A**. Note the crystals with growth discontinuities (arrows). Although the entire rocks have been dolomitized, the relic fabrics of the original aragonite crystals are retained. (**F**) Divergent fabrics of dolomite crystals with sweeping extinction under XPL in labelled rectangles in **A**. (**G**) Dolostone slab 14AD-4 with crystal fans growing above dolomitic sediments. Scale in millimeters. (**H-I**) Closer views of crystal fans in labelled rectangles in **G**, showing growth discontinuities (arrows in **I**) within the aragonite crystals. PPL: plane polarized light; XPL: cross polarized light.

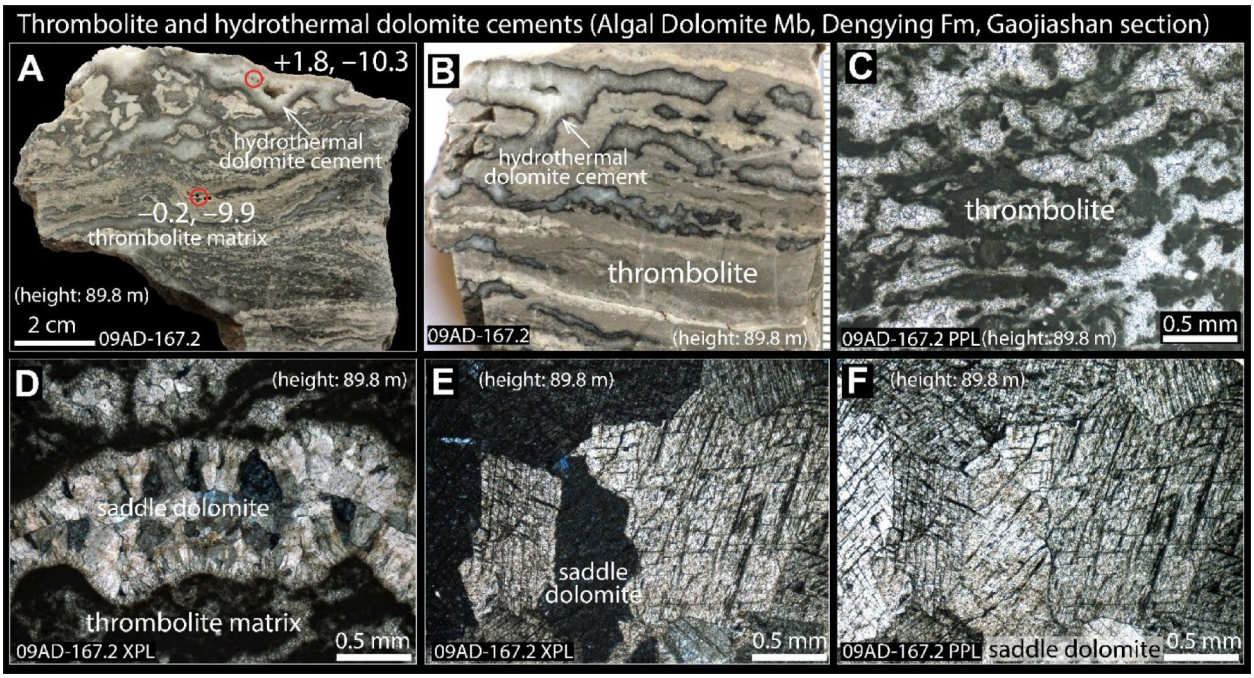

Figure 5.

Thrombolitic dolostone and void-filling hydrothermal dolomite cements in the Algal Dolomite Member, Dengying Formation, at the Gaojiashan section. Sample 09AD-167.2 with a stratigraphic height of 89.8 m in Fig. 12. (**A-B**) Dolostone slabs showing thrombolitic dolomite matrix with vug-filling dolomite cements. Fabric-specific $\delta^{13}C$ (left) and $\delta^{18}O$ (right) data are provided in A. Scale in **B** in millimeters. (**C**) A closer view of the thrombolitic dolomite matrix under plane polarized light. (**D**) A closer view of coarse dolomite cements in the thrombolitic dolomite matrix under cross polarized light. (**E, F**) Closer views of hydrothermal saddle dolomites with two distinct sets of cleavages and sweeping extinction. PPL: plane polarized light; XPL: cross polarized light.

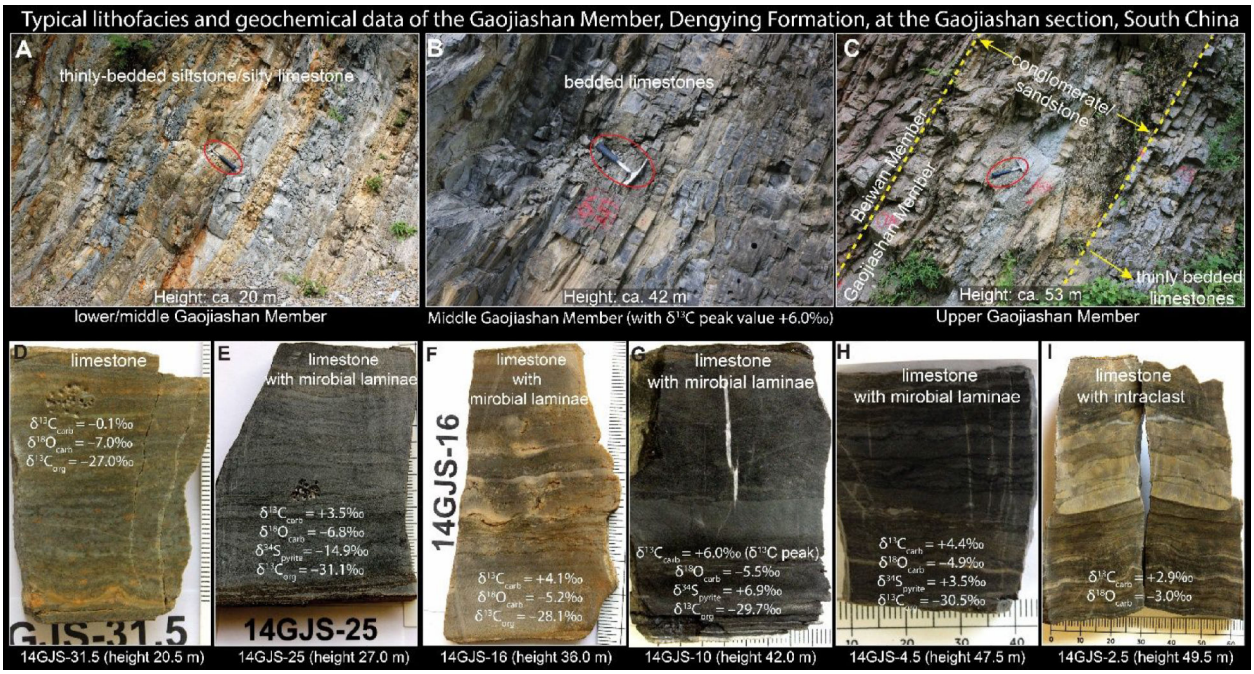

Figure 6.

Typical lithofacies and geochemical data of the Gaojiashan Member, Dengying Formation, at the Gaojiashan section. Stratigraphic height numbers representing the distance above the Algal Dolomite/Gaojiashan boundary. (**A**) Thinly bedded siltstones and silty limestones at the lower/middle transition of the Gaojiashan Member. (**B**) Dark-colored thin-bedded limestones in the middle Gaojiashan Member that records a $\delta^{13}C_{carb}$ positive excursion up to +6‰ (Cui et al., 2016b). (**C**) A conglomerate/sandstone interval in the upper Gaojiashan Member. (**D-I**) Photos of freshly cut slabs of samples from the Gaojiashan Member with microbial laminae and intraclasts. These slabs represent greenish grey dolostone (**D**), limestones with microbial laminae (**E-H**), and intraclastic limestone (**I**). The numbers in the sample IDs represent distance (in meters) below the conglomerate interval in the upper Gaojiashan Member. For example: sample 14GJS-10 is 10 m below the conglomerate interval in the Gaojiashan Member. The $\delta^{13}C_{carb}$ and $\delta^{18}O_{carb}$ values of micro-drilled carbonate powders are marked on the slab. The $\delta^{34}S_{pyrite}$ and $\delta^{13}C_{org}$ values of each slab were analyzed from bulk acidified residues.

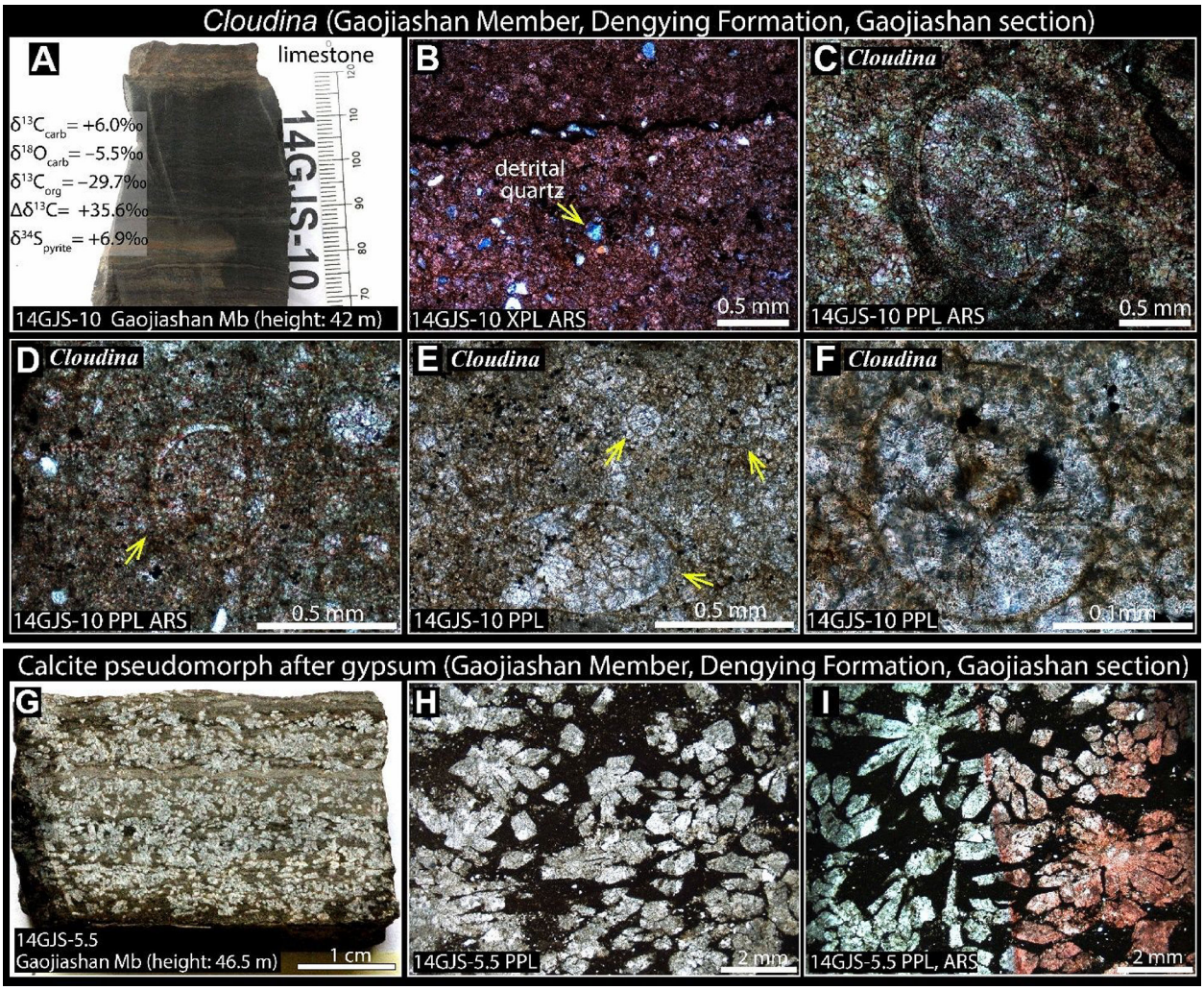

Figure 7.

Fossils and gypsum pseudomorphs in the Gaojiashan Member, Dengying Formation, at the Gaojiashan section. (**A**) Limestone slab 14GJS-10 (collected at 42 m in Fig. 13) with the terminal Ediacaran fossil *Cloudina.* (**B**) Thin section of 14GJS-10 stained by Alizarin Red S, confirming its limestone lithology. Note abundant detrital quartz in this sample (arrow). (**C-F**) Transverse cross sections of *Cloudina* (arrows) in thin sections of the sample 14GJS-10. (**G**) Rock slab of sample 14GJS-5.5 (collected at 46.5 m in Fig. 13), showing calcite pseudomorphs after gypsum in the Gaojiashan Member. (**H-I**) Closer views of the calcite pseudomorphs after gypsum rosettes. The right half of image **I** shows a red color after being stained by Alizarin Red S, confirming the calcite composition of the pseudomorphs. PPL: plane polarized light; XPL: cross polarized light. ARS: stained by Alizarin Red S.

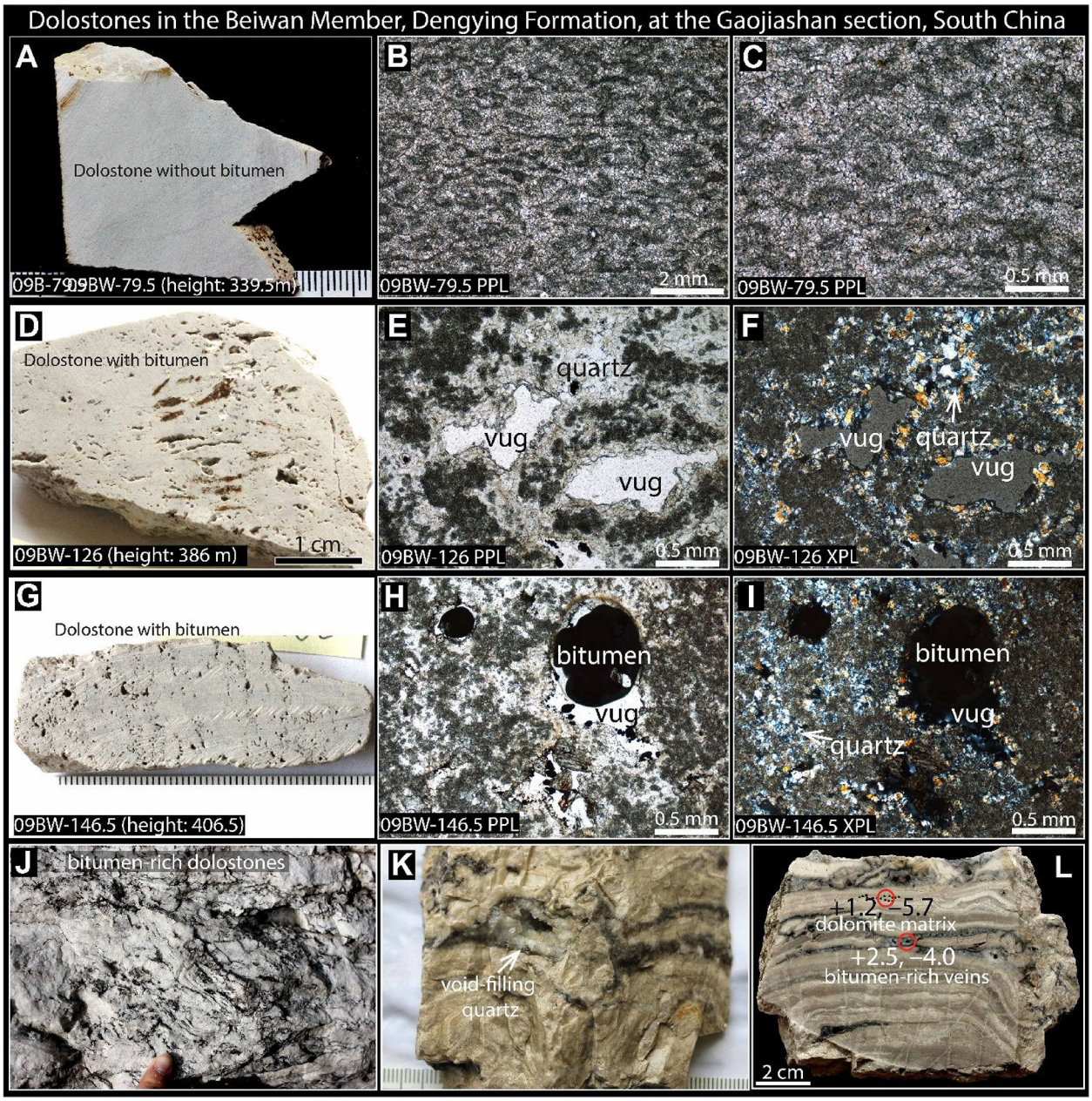

Figure 8.

Petrographic observations of dolostones in the Beiwan Member, Dengying Formation, at the Gaojiashan section. (**A-C**) Slab and petrographic photos of sample 09BW-79.5 (collected at 339.5 m in Fig. 12) showing dolomicrite with abundant algal fabrics (?). (**D-F**) Slab and petrographic photos of sample 09BW-126 (collected at 386 m in Fig. 12) showing dolostone with vugs and quartz cements. (**G-I**) Slab and petrographic photos of sample 09BW-146.5 (collected at 406.5 m in Fig. 12). Note the vugs with bitumen in **H** and **I**, and the quartz cements (arrows) in **F** and **I** under cross polarized light. (**J**) Outcrop photograph showing dolostones (white) with abundant bitumen (black). (**K, L**) Photographs of hand samples, showing bitumen in dissolution vugs. Note the void-filling quartz (arrow) in **K**. Micro-

drilling geochemical $\delta^{13}C$ (left) and $\delta^{18}O$ (right) data are provided in **L**. PPL: plane polarized light; XPL: cross polarized light.

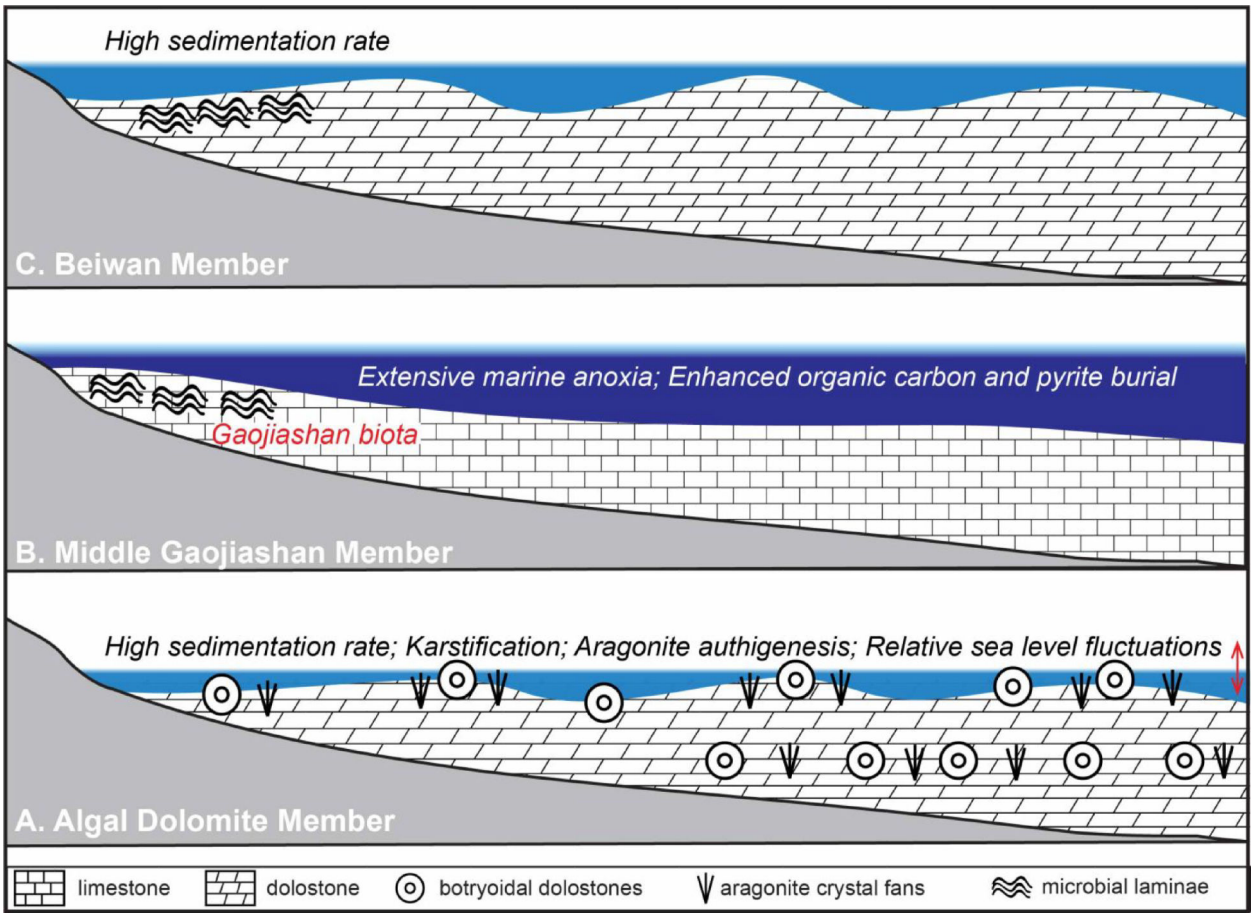

Figure 9.

A depositional model of the terminal Ediacaran Dengying Formation based on studies of the Gaojiashan section. See main text for a detailed discussion.

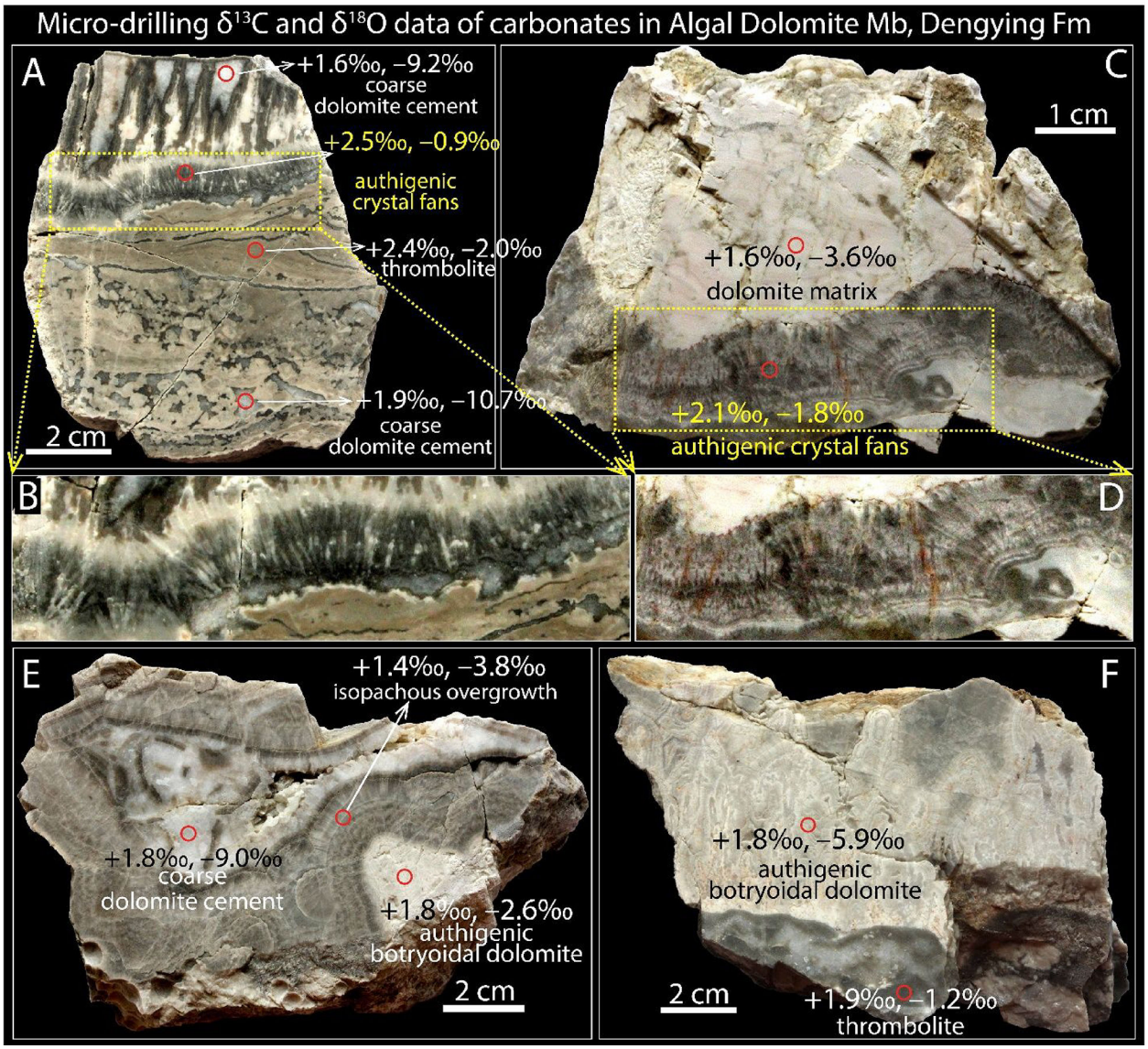

Figure 10.

Carbonate $\delta^{13}C$ (left) and $\delta^{18}O$ (right) values of micro-drilled samples from the Algal Dolomite Member, Dengying Formation, at the Gaojiashan section. (**A-D**) Freshly cut dolostone slabs showing authigenic crystal fans. A and B also illustrated in Fig. 4A–F; C and D also illustrated in Fig. 4G–I. Although all samples have been dolomitized, relic fabrics of aragonite are retained. (**E-F**) Freshly cut dolostone slabs showing thrombolite matrix, botryoidal dolomite, isopachous cements, and late-stage dolomite cements. Note the relatively high $\delta^{18}O_{carb}$ values in the aragonite crystal fans (−0.9‰ in A and −1.8‰ in C) and the relatively low $\delta^{18}O_{carb}$ values in the late-stage coarse dolomite cements (−9.2‰ in A and −9.0‰ in E).

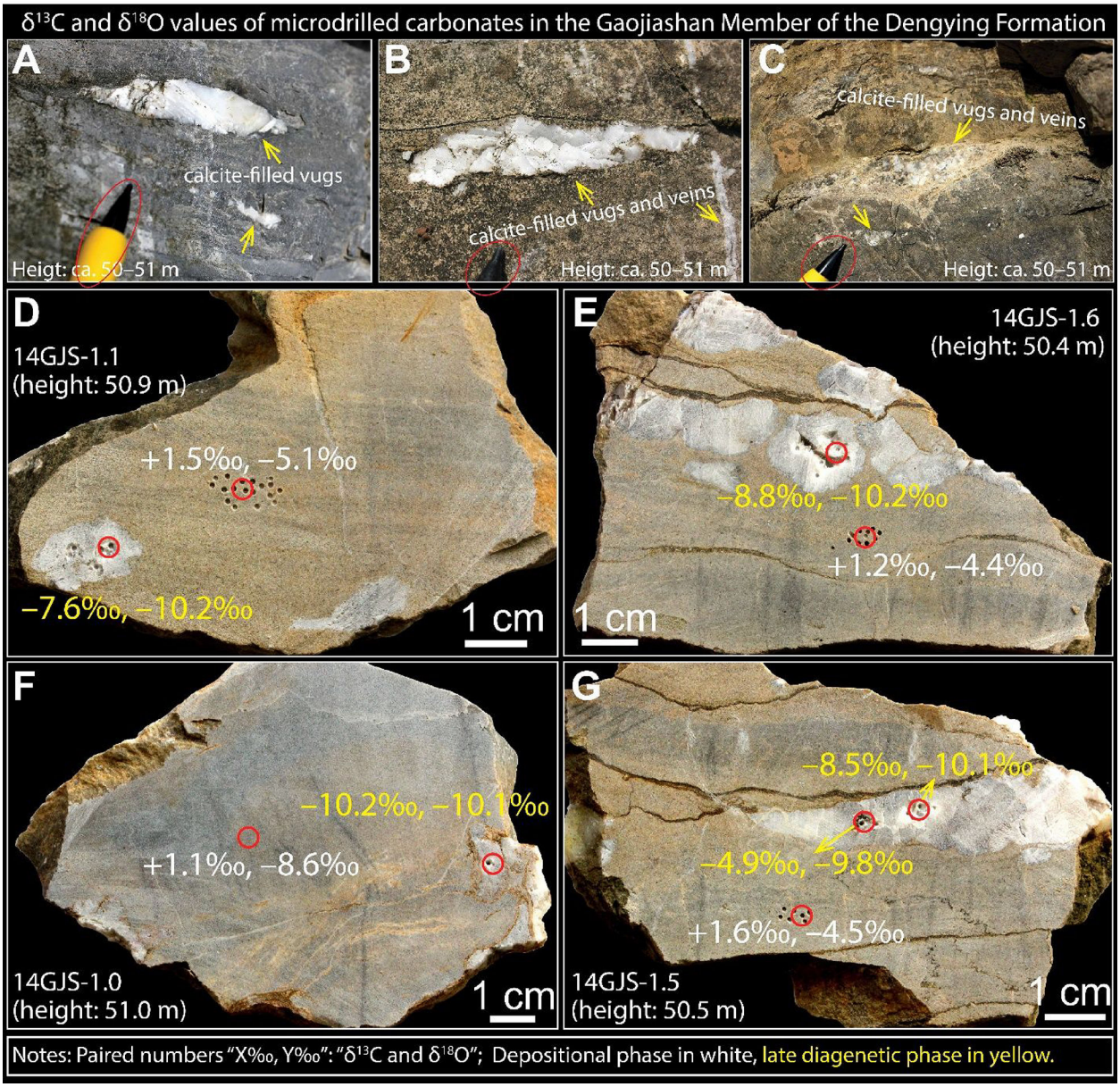

Figure 11.

Carbonate $\delta^{13}C$ (left) and $\delta^{18}O$ (right) values of micro-drilled samples from the Gaojiashan Member, Dengying Formation, at the Gaojiashan section. (**A-C**) Calcite-filled vugs and veins (arrows) at ca. 50–51 m in Fig. 13. Pencil for scale. (**D-G**) Carbonate $\delta^{13}C$ (left) and $\delta^{18}O$ (right) values of micro-drilled samples from the Gaojiashan Member. Note that the $\delta^{13}C$ and $\delta^{18}O$ values (in yellow) of the vug-filling calcite are consistently lower than those (in white) measured from the host carbonate rocks. Numbers in sample IDs represent distance (in meters) below the conglomerate/sandstone interval of the upper Gaojiashan Member. The stratigraphic height values in D-G representing the distance above the Gaojiashan/Algal Dolomite boundary.

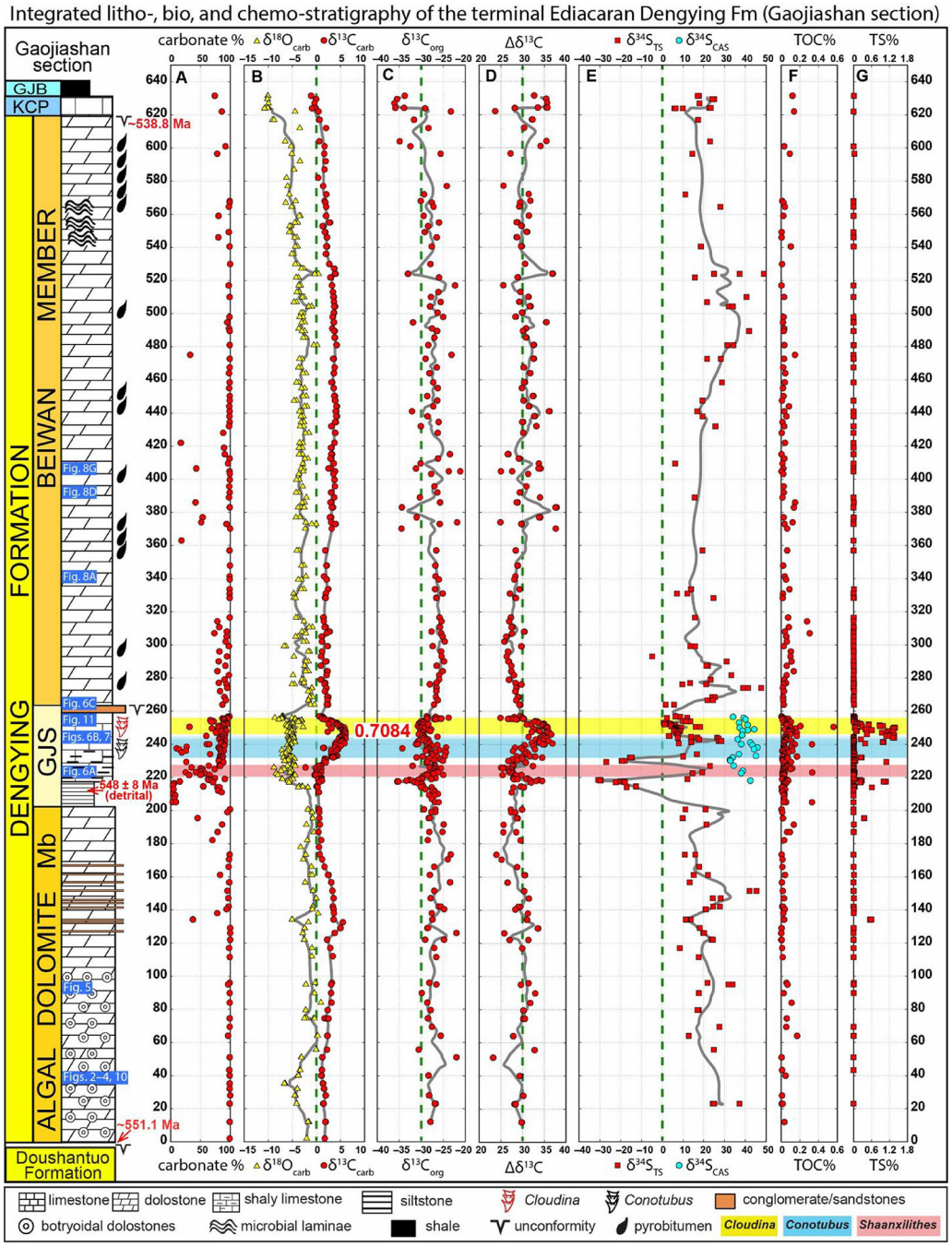

Figure 12.

Integrated litho-, bio-, and chemo-stratigraphy of the terminal Ediacaran Dengying Formation at the Gaojiashan section. Geochemical profiles showing the data of carbonate contents, carbonate carbon isotopes ($\delta^{13}C_{carb}$, ‰ V-PDB), carbonate oxygen isotopes ($\delta^{18}O_{carb}$, ‰ V-PDB), organic carbon isotopes ($\delta^{13}C_{org}$, ‰ V-PDB), carbon isotope fractionations ($\Delta\delta^{13}C_{carb\text{-}org}$), pyrite sulfur isotopes ($\delta^{34}S_{TS}$, ‰ V-CDT), carbonate associated sulfate (CAS) sulfur isotopes ($\delta^{34}S_{CAS}$, ‰ V-CDT), total organic carbon content (TOC), and total sulfur content (TS, dominated by pyrite with trace amount of organic S) of

acidified residues. The gray lines representing the five-point running average of the chemostratigraphic data. The lowest $^{87}Sr/^{86}Sr$ value (0.7084) measured from a limestone sample in the Gaojiashan Member is also makred in the $\delta^{13}C_{carb}$ profile (at 246 m in stratigraphic height). The stratigraphic positions of some figures have been marked on the lithology column. Note that $\delta^{13}C_{carb}$ and $\delta^{18}O_{carb}$ data plotted here and in Figs. 13, 14 only include micro-drilled samples of the least-altered micritic carbonate matrix, whereas $\delta^{13}C_{org}$ and $\delta^{34}S_{TS}$ data were measured from bulk samples after a complete acidification of carbonates. TS and TOC data are generally low due to significant carbobonate dilutions. Source of the detrital ziron age: (Cui et al., 2016b). Abbreviations: GJS = Gaojiashan Member, KCP = Kuanchuanpu Formation, GJB = Guojiaba Formation. See the online supplementary material for the complete data.

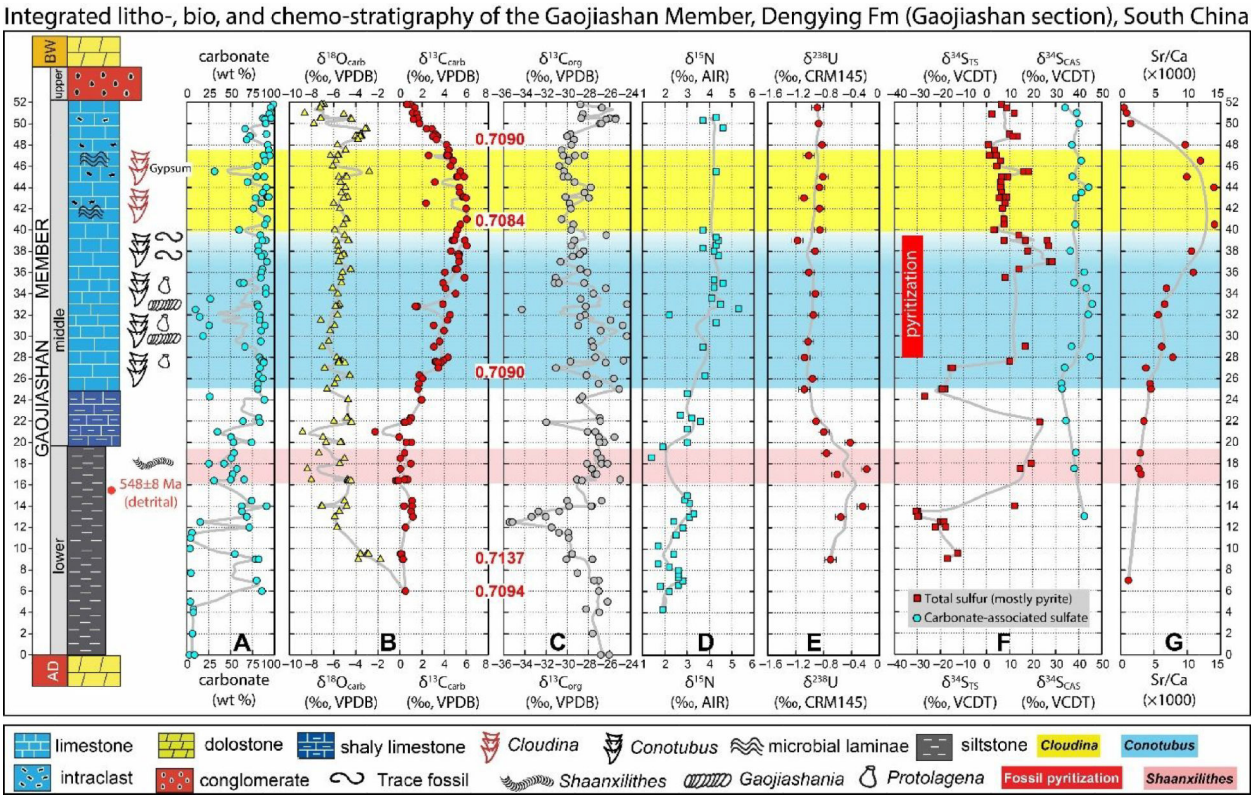

Figure 13.

Integrated litho-, bio-, and chemo-stratigraphy of the Gaojiashan Member of the middle Dengying Formation at the Gaojiashan section. Geochemical profiles showing the data of carbonate contents (wt. %), carbonate carbon isotopes ($\delta^{13}C_{carb}$, ‰ V-PDB), carbonate oxygen isotopes ($\delta^{18}O_{carb}$, ‰ V-PDB), organic carbon isotopes ($\delta^{13}C_{org}$, ‰ V-PDB), nitrongen isotopes ($\delta^{15}N$, ‰ AIR), uranium isotopes ($\delta^{238}U$, ‰ CRM145), sulfur isotopes ($\delta^{34}S_{TS}$, ‰ V-CDT) of total sulfur (TS, dominated by pyrite with trace amount of organic S) after a complete acidification of carbonates, carbonate associated sulfate (CAS) sulfur isotopes ($\delta^{34}S_{CAS}$, ‰ V-CDT), Sr and Ca concentration (in ppm) ratios (Sr/Ca). Gray lines represent three-point running average of the chemostratigraphic data. $^{87}Sr/^{86}Sr$ values measured from limestone beds or limestone nodules in the Gaojiashan Member are also makred along the $\delta^{13}C_{carb}$ profile. Data source: $\delta^{13}C$, $\delta^{18}O$, $\delta^{34}S$, Sr/Ca data (Cui, 2015; Cui et al., 2016b), $^{87}Sr/^{86}Sr$ values (this study), $\delta^{15}N$ data (Gamper, 2014), $\delta^{238}U$ data (Zhang et al., 2018). Modified from (Cui et al., 2016b).

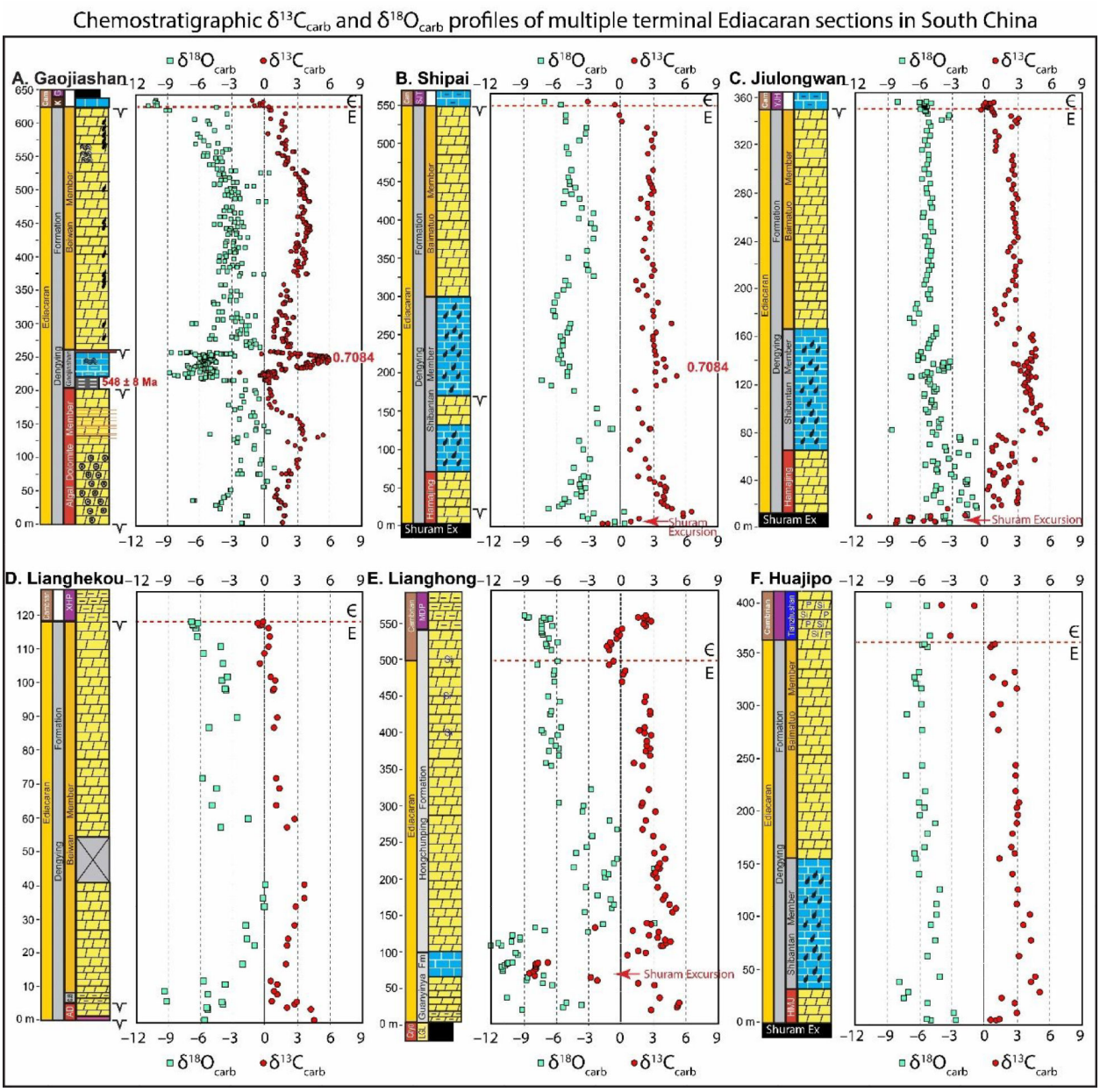

Figure 14.

Chemostratigraphic $\delta^{13}C_{carb}$ (‰, V-PDB) and $\delta^{18}O_{carb}$ (‰, V-PDB) profiles of multiple terminal Ediacaran sections in South China. Data source: (**A**) Gaojiashan section (this study); (**B**) Shipai section (Jiang et al., 2007); (**C**) Jiulongwan section (Wang et al., 2014a); (**D**) Lianghekou section (Chen et al., 2015); (**E**) Lianghong section (Wang et al., 2012); (**F**) Huajipo section (Zhang et al., 2004). Source of the lowest $^{87}Sr/^{86}Sr$ values (0.7084): Gaojiashan section (this study) and Shipai section (Jiang et al., 2007). Abbreviations: Shuram Ex = Shuram Excursion. AD = Algal Dolomite Member, GJS = Gaojiashan Member, XHP = Xihaoping Member, MDP = Maidiping Formation, YJH = Yanjiahe Formation, K = Kuanchuanpu Formation, G = Guojiaba Formation, Cam = Cambrian, E = Ediacaran, <MI> = Cambrian.

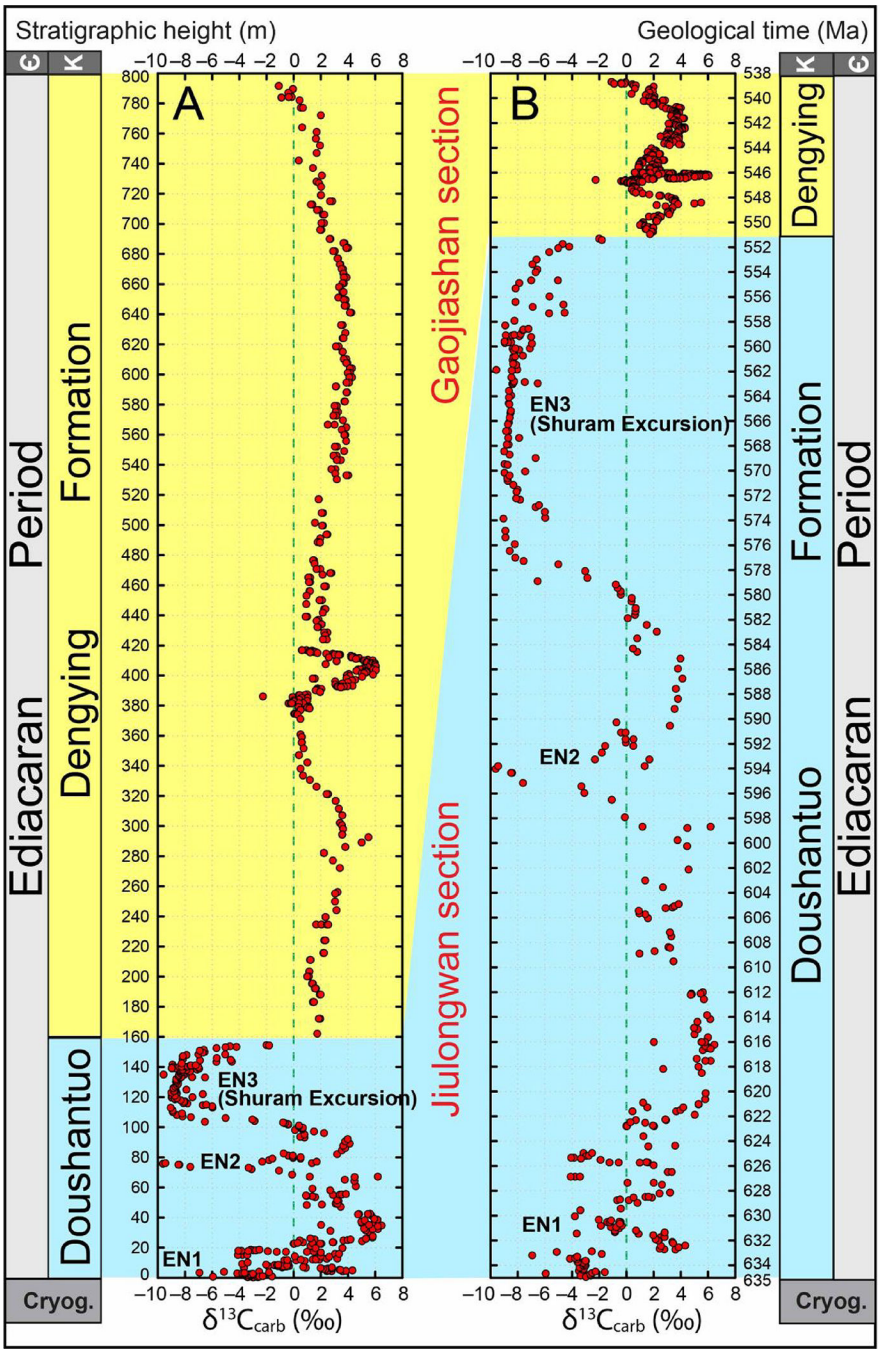

Figure 15.

$\delta^{13}C_{carb}$ (‰, V-PDB) chemostratigraphic data of the Ediacaran Period in South China plotted against (**A**) stratigraphic height and (**B**) estimated geological time. Data source: Doushantuo Formation at the Jiulongwan section (Jiang et al., 2007; McFadden et al., 2008); Denging Formation at the Gaojiashan section (Cui, 2015; Cui et al., 2016b). Abbreviations: K = Kuanchuanpu Formation, <MI> = Cambrian, Cryog. = Crogenian Period. EN = Ediacaran $\delta^{13}C_{carb}$ Negative excursions. See the main text for detailed discussion.